HHS Public Access

Author manuscript

Cell Rep. Author manuscript; available in PMC 2022 December 28.

Published in final edited form as:

Cell Rep. 2022 November 15; 41(7): 111658. doi:10.1016/j.celrep.2022.111658.

Development of single-molecule ubiquitination mediated fluorescence complementation to visualize protein ubiquitination dynamics in dendrites

Marius F. Ifrim[1,2,3,*], **Aleksandra Janusz-Kaminska**[2], **Gary J. Bassell**[2,*]

[1]Department of Cell and Developmental Biology, State University of New York, Upstate Medical University, Weiskotten Hall, 766 Irving Avenue, Syracuse, NY 13210, USA

[2]Department of Cell Biology, Emory University School of Medicine, 615 Michael St., Atlanta, GA 30322, USA

[3]Lead contact

SUMMARY

The ubiquitination/proteasome system is important for the spatiotemporal control of protein synthesis and degradation at synapses, while dysregulation may underlie autism spectrum disorders (ASDs). However, methods allowing direct visualization of the subcellular localization and temporal dynamics of protein ubiquitination are lacking. Here we report the development of Single-Molecule Ubiquitin Mediated Fluorescence Complementation (SM-UbFC) as a method to visualize and quantify the dynamics of protein ubiquitination in dendrites of live neurons in culture. Using SM-UbFC, we demonstrate that the rate of PSD-95 ubiquitination is elevated in dendrites of *FMR1 KO* neurons compared with wild-type controls. We further demonstrate the rapid ubiquitination of the fragile X messenger ribonucleoprotein, FMRP, and the AMPA receptor subunit, GluA1, which are known to be key events in the regulation of synaptic protein synthesis and plasticity. SM-UbFC will be useful for future studies on the regulation of synaptic protein homeostasis.

In brief

Ifrim et al. use single-molecule imaging of reconstituted split-Venus fluorescent protein to visualize protein specific *de novo* ubiquitination events in live cells, with the ability to observe global ubiquitination rate differences between WT and *Fmr1* KO neurons and to detect global ubiquitination rate changes after mGluR activation.

Graphical Abstract

*Correspondence: ifrimm@upstate.edu (M.F.I.), gbassel@emory.edu (G.J.B.).

AUTHOR CONTRIBUTIONS

M.F.I., A.J.-K., and G.J.B. designed the research; M.F.I. and A.J.-K. performed the research; M.F.I. and A.J.-K. analyzed the data; M.F.I., A.J.-K., and G.J.B. wrote the paper.

DECLARATION OF INTERESTS

G.J.B. serves on advisory board of *Cell* Reports.

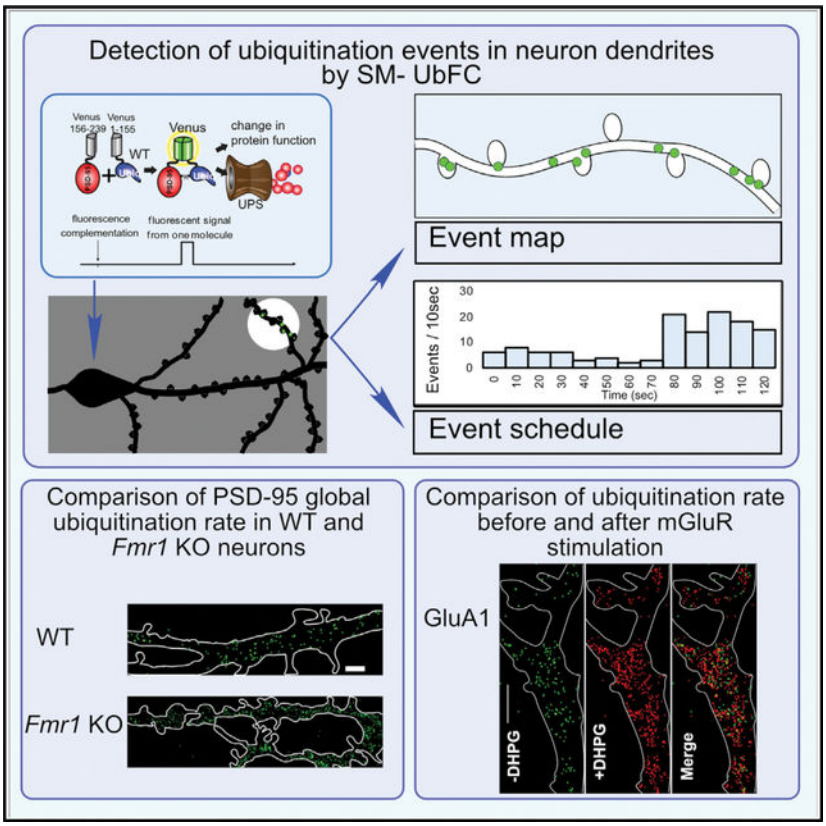

INTRODUCTION

It has been long recognized that normal synaptic function depends on maintaining protein homeostasis at the synapse (Steward and Schuman, 2003; Bingol and Schuman, 2006; Tai and Schuman, 2008). Tight spatial and temporal control of both synaptic protein synthesis and degradation is believed to be required for normal synaptic function. Conversely, altered regulation of the balance between protein synthesis and degradation may underlie diseases, such as autism spectrum disorders (ASDs) and other neurodevelopmental disorders. In a mouse model of fragile X syndrome (FXS) it has been reported that not only is protein synthesis dysregulated (Ifrim et al., 2015), but also the ubiquitination of several synaptic proteins is altered with consequences on synapse stability (Tsai et al., 2012). Both ubiquitin and the proteasome are present in dendrites, in the proximity of active synapses (Patrick et al., 2003), suggesting that synaptic proteins might be ubiquitinated and degraded in spines or dendrites. It has also been shown that biochemically isolated synaptic fraction contains the enzymatic machinery necessary for ubiquitin conjugation to substrates and that the degradation of the synaptic proteins is dependent on the levels of glutamate receptor activation (Ehlers, 2003). The ubiquitin-proteosome system was shown to be necessary for the rapid, ligand-induced endocytosis of AMPA receptors. Using microscopy methods, these authors observed a proteasome-dependent decrease in dendritic Postsynaptic Density Protein 95 (PSD-95); however, biochemical analysis precluded the detection of polyubiquitinated PSD-95 (Patrick et al., 2003). It was concluded that the polyubiquitination of PSD-95 may

be short-lived and thus difficult to detect, which necessitates the development of alternative methods. In another study, the ubiquitination of PSD-95 by the E3 ligase Mdm2 was found to be necessary for the NMDA dependent internalization of AMPA receptors (Colledge et al., 2003). Here the ubiquitination of PSD-95 was transiently detected in whole-cell lysates following 10-min NMDA treatment. The rapid ubiquitination of AMPA receptor subunits GluA1 and GluA2 has also been shown to be necessary for ligand-induced trafficking to late endosomes (Widagdo et al., 2015). The fragile X messenger ribonucleoprotein, FMRP, is another protein known to be ubiquitinated in response to the gp1 mGlu agonist, DHPG ((S)-3,5-Dihydroxyphenylglycine hydrate) (Nalavadi et al., 2012; Hou et al., 2006).

While these and other studies document the importance of the ubiquitination and proteasome system in synaptic protein homeostasis and neuronal function (Lin and Man, 2013), the methods used do not allow for the direct visualization of subcellular localization and dynamics of ligand-induced ubiquitination. The transient nature of the ubiquitinated products hinders their detection and prevents the analysis of the rate and how the rate of protein ubiquitination may be affected by synaptic plasticity and/or altered in neurodevelopmental disorders. Synaptic protein homeostasis likely requires local adjustments of the ubiquitination rate, appropriate for the stimulation received locally, which may be altered during synaptic plasticity.

Because ubiquitination involves the formation of a stable, covalent bond between a lysine residue of the target protein and a ubiquitin molecule, the widely used bimolecular fluorescence complementation (BiFC) (Hu et al., 2002) was adapted to visualizing ubiquitinated proteins by ubiquitin mediated fluorescence complementation (Ub-FC) (Fang and Kerppola, 2004). Both the target protein and ubiquitin are fused to different halves of YFP, and the fluorescent signal of YFP is detected only when the target protein (tagged) is ubiquitinated by a tagged ubiquitin. Because of the formation of the covalent bond by ubiquitination, the halves of YFC are held in close proximity and YFP is reconstituted and becomes fluorescent. The original Ub-FC method requires a large number of ubiquitinated protein molecules to accumulate in order for the fluorescence to be detected and thus allows for visualization of steady-state levels of a ubiquitinated protein in live cells. The location where the ubiquitination takes place, its dynamic regulation by physiologic stimuli, or the ubiquitination rate cannot be determined therefore by this method.

Advances in single-molecule imaging techniques and the ability to detect molecular interactions in live cells have provided new insights in molecular and spatiotemporal dynamics that are not possible to infer from steady-state or bulk measurements. Recent studies have used single-molecule imaging of a Venus-based fluorescent reporter to enable the direct visualization of translation events allowing detection close to the translation site (Ifrim et al., 2015; Tatavarty et al., 2012; Xie et al., 2008). Here we report the adaptation of this single-molecule imaging technology using Venus for visualizing *de novo* ubiquitination events in live neurons with high spatial and temporal resolution. We refer to this method as Single-Molecule Ubiquitination Mediated Fluorescence Complementation (SM-UbFC), which uses single-molecule imaging of reconstituted split Venus generated by ubiquitin mediated fluorescence complementation (Fang and Kerppola, 2004). SM-UbFC combines the advantages of single-molecule detection of Venus fluorescence protein in live neurons

(Tatavarty et al., 2012) with those of UbFC (Fang and Kerppola, 2004). The biophysical properties of Venus, which has a fast maturation time and fast photobleaching kinetics, make it ideal for single-molecule imaging. We used SM-UbFC to visualize and quantify the dynamics of FMRP and GluA1 protein ubiquitination in dendrites in response to plasticity-inducing stimuli, and PSD-95 ubiquitination impairments in a mouse model of FXS. These examples provide proof-of-principle demonstration that this methodology will open the door for addressing important questions on the spatiotemporal dynamics of protein ubiquitination that are broadly relevant to synapse biology in health and disease.

RESULTS

PSD-95 ubiquitination was visualized in dendrites of live neurons using SM-UbFC

We first used SM-UbFC to directly visualize *de novo* the ubiquitination of PSD-95 in dendrites of cultured hippocampal neurons owing to knowledge of the mechanism of ubiquitination and availability of control reagents to validate this method (Colledge et al., 2003; Bianchetta et al., 2011). PSD-95 is a postsynaptic scaffolding protein, which anchors NMDA and AMPA receptors and plays important roles in synaptic plasticity.

To perform SM-UbFC, we generated split-Venus fluorescent protein constructs for PSD-95 and ubiquitin, instead of using split-YFP (Figure 1A). Venus is a fast-folding, fast-bleaching variant of YFP, which we used previously for single-molecule imaging of protein translation in live neurons (Barbarese et al., 2013; Ifrim et al., 2015; Tatavarty et al., 2012). The fast-bleaching kinetics of Venus allows for only minimal accumulation of Venus fluorescence during imaging, with the appearance of sparse flashes of light, on a black background, corresponding to newly maturated Venus molecules. This permitted single-molecule detection, which in turn allows for nanometer spatial resolution and 150-ms temporal resolution. By applying the same principle to ubiquitination, we predicted that *de novo* ubiquitination events could be detected in live cells. The above constructs were transfected in cultured hippocampal neurons (14 DIV) and incubated to allow for protein expression. Time-lapse imaging of live cells was performed as described in the STAR Methods section. Transfected neurons showed Venus fluorescence throughout the soma and dendrites. After the bleaching of the initial fluorescence under imaging conditions using laser excitation, sparse flashes of light were detected on a dark background, corresponding to ubiquitination events. The flashes of light displayed a one-step appearance (reconstitution of Venus), one-step disappearance (Venus photobleaching), and constant level of fluorescence from appearance to disappearance consistent with single-molecule behavior (Figure 1B). Events could be observed appearing and disappearing one near another one, with little movement, which allowed for the identification of individual molecules by the particle-tracking algorithms (Figure 1C). Each reconstituted Venus molecule detected was tracked from appearance (maturation) to disappearance (bleaching). For each molecule detected, the centroid coordinates and timing of the first appearance were recorded. The analysis software is available at https://health.uconn.edu/yu-lab/software/. To visualize the location of new ubiquitination events in dendrites, an *Event Map* (Figure 1D) was built by plotting the centroid coordinates for all the events detected in the region of interest (ROI) over a time interval. Using this method, PSD-95 ubiquitination was detected in

dendrites and spines (Figure 1D). When analyzing dendritic segments (>40 μm from the cell body), PSD-95 ubiquitination events were detected throughout the dendrites, with some regions showing more clustering (Figure 1D). Using immunofluorescence to detect the 20S proteasome subunit, which was performed after the live cell experiments (Figure 1E), PSD-95 ubiquitination events in dendrites were often near but not direly colocalized with 20s proteasome puncta (Figure 1F, arrow). Less frequently PSD-95 ubiquitination events were colocalized with 20s proteasome in dendrites (Figure 1F, arrowhead). We analyzed the photobleaching kinetics of PSD-95 using SM-UbFC in live neurons and observed that most of the flashes disappear in less than a second, matching the photobleaching kinetics of Venus as determined in other studies (Figure 1H) (Yu et al., 2006; Tatavarty et al., 2012). These results confirm that the flashes of light represent reconstituted Venus molecules. Furthermore, we compared the fluorescence intensity of the flashes of light observed in SM-UbFC experiments in live cells with that of full-length Venus expressed in live cells and also with that of purified Venus *in vitro* (Figure 1I). The distribution of fluorescence intensities is similar in all the three conditions, further confirming that the light flashes represent reconstituted Venus molecules.

PSD-95 SM-UbFC signal is specific for ubiquitination

To confirm that the signal detected is specific for the ubiquitination of PSD-95, we performed several control experiments. For these control experiments, we used N2A cells as a more tractable experimental system, instead of hippocampal neurons, owing to the higher transfection efficiency and less variability. To determine if the reconstitution of split Venus, and thus the signal detected, is specific for the ubiquitination of PSD-95, SM-UbFC signal was analyzed when the G76A mutation in ubiquitin was introduced, which is known to inhibit the incorporation of ubiquitin in ubiquitinated products (~4-fold decrease) (Pickart et al., 1994) (Figure 2A). When SM-UbFC was performed in N2A cells using BiFC-PSD-95 wild type (WT) and BIFC-Ub G76A, a marked reduction in the ubiquitination rate was observed (Figures 2A–2C) compared with BiFC-PSD-95 WT and BIFC-Ub WT. When SM-UbFC was performed in N2A cells using BiFC-PSD-95 WT and BIFC- ΔUbiq an even higher reduction in the ubiquitination rate was observed (Figures 2A–2C). To determine if the SM-UbFC signal reflects direct ubiquitination of PSD-95, the converse experiment was performed, using BiFC-PSD-95 Lys Mut (in which five known ubiquitination sites were mutated to alanine [Bianchetta et al., 2011]). When SM-UbFC was performed in N2A cells using the BiFC-PSD-95 Lys Mut, a significant reduction in signal was observed, as expected, supporting the interpretation that the observed signal is specific for direct PSD-95 ubiquitin interaction (Figures 2D–2F). To further confirm that the flashes of light detected represent ubiquitination events, SM-UbFC was performed in the presence of drugs that inhibit either Mdm2 (PSD-95E3 ubiquitin ligase) or the proteasome. When PSD-95 ubiquitination rate was measured in the presence of Mdm2 inhibitor HLI373 (Kitagaki et al., 2008), the rate at which the flashes of light were detected decreased, as expected, in comparison with vehicle treatment, confirming that SM-UbFC events represent PSD-95 ubiquitination events (Figures 2G and 2H). Inhibition of the proteasome with MG132 did not result in a significant change of the ubiquitination rate; however, a decreased trend was observed. This might be explained by the accumulation of ubiquitinated products, following

the inhibition of the ubiquitin proteasome system. Such accumulation would determine a slower rate for further ubiquitination (the equilibrium is pushed toward less ubiquitination).

Biochemical analysis confirms WT and mutant plasmids used are expressed at similar levels

To confirm that the decrease in the ubiquitination rate observed with ubiquitin and PSD-95 mutants is due to the effect of the mutations on the ubiquitination rates and not due to differential expression, we performed biochemical experiments. Because the PSD-95 constructs do not have an epitope tag, we used SH-SY5Y cells, which express endogenous PSD-95 at much lower levels than N2A cells (Figure 3A). When SH-SY5Y cells were transfected with plasmids expressing either BiFC-PSD-95 WT or BiFC-PSD-95 Lys Mut and Scarlet-I for transfection control and analyzed by western blot, we found that the expression levels of BiFC-PSD-95 WT and BiFC-PSD-95 Lys Mut do not differ (Figures 3B–3D).

To determine if BiFC-Ub G76A mutant is indeed less present in ubiquitinated proteins than BiFC-Ub WT, and whether it affects the overall ubiquitination levels due to its possible suppression of deubiquitylation, SH-SY5Y cells were transfected with plasmids expressing either BiFC-Ub WT or BiFC-Ub G76A mutant and Scarlet-I for transfection control and analyzed by western blot. BiFC-Ub G76A mutant was much less associated with high molecular weight ubiquitinated protein species than BiFC-Ub WT and instead shows less ubiquitinated protein species and bands that presumably correspond to self-polymerized ubiquitin (Hodgins and Ellison, 1992), (red boxes) (Figure 3E). When the same lysates of cells transfected with BiFC-Ub WT, BiFC-Ub G76A mutant, or mock transfected, were analyzed by western blot probed for ubiquitin and GAPDH, we observed no significant change total ubiquitinated protein levels in the cell, or change in the ubiquitination profiles (Figures 3F and 3G). Figures 3E and 3F show a parallel western blot performed on the same samples.

To confirm that BiFC-Ub WT can physically “conjugate” BiFC-PSD-95 WT, GFP-Trap pull-down analysis was used. GFP-Trap pull-down analysis is based on pull down by GFP-Trap nanobody of reconstituted BiFC Venus. GFP-Trap nanobody does not bind to either half of Venus alone and pulls down only the complemented Venus protein (Croucher et al., 2016) (Figure 3H). SH-SY5Y cells were transfected with plasmids expressing BiFC-PSD-95 and either BiFC-Ub WT or BiFC-Ub G76A (the latter two containing an HA-tag). After overnight expression, lysates were subjected to pull down with GFP-Trap magnetic beads, then analyzed by the western blot. The lysates were analyzed by western blot probed for HA-tag, PSD-95, and GAPDH (Figure 3I). When the GFP-Trap pull-down fraction from the same experiment was analyzed by western blot probed for HA-tag and PSD-95, a PSD-95 positive band, running higher than the BiCF-PSD95 in the lysate was observed and this band is stronger in the G76A Ubiq mutant (Figure 3J). Since only BiFC-conjugated ubiquitinated PSD-95 species were pulled down, we suspect that it is a mono-ubiquitinated tagged PSD-95. High molecular species complexes detected by anti-HA are present in the BiFC-PSD-95 WT/BiFC-Ub WT lane, but not in the BiFC-PSD-95 WT/BiFC-Ub G76A lane (Figure 3J). Taken together, these suggest BiFC-Ub WT can effectively conjugate with

its substrate, while BIFC-Ub G76A is not efficiently used for ubiquitination, and these findings are consistent with our interpretation of imaging data.

PSD-95 ubiquitination rate is increased in dendrites of *Fmr1* KO neurons

Excess and dysregulated mRNA translation is a well-characterized feature of FXS. However, recently, defects in protein ubiquitination have been reported in FXS, including PSD-95 ubiquitination (Tsai et al., 2012; Liu et al., 2017). PSD-95 ubiquitination has been shown to be modulated by NMDA signaling and to be required for AMPA receptor endocytosis following NMDAR stimulation in a cLTD paradigm (cLTD-chemical long-term depression) (Ma et al., 2017). These studies underscore the known role of PSD-95 in long-term depression (LTD) (Colledge et al., 2003; Xu et al., 2008; Bhattacharyya et al., 2009; Kim et al., 2007).

Using a full-length Venus-PSD-95 reporter (contains full open reading frame and 3′UTR) to quantify single-molecule translation, we previously observed elevated PSD-95 translation rates in *Fmr1* knockout (KO) compared with WT neurons (Ifrim et al., 2015), consistent with loss of FMRP-mediated repression of translation. We hypothesized that there may be also an elevated ubiquitination rate, perhaps as a compensatory response to excess translation. This would be a good model system to further valuate this method. Using the same PSD-95-3-UTR reporter as used previously with full-length Venus, here we used SM-UbFC to compare basal ubiquitination rate of PSD-95 in dendrites of WT and *Fmr1* KO neurons. WT or *Fmr1* KO neurons at 14DIV were transfected and imaged as mentioned previously. The data were analyzed as previously described for Figure 1 and event maps were constructed (Figures 4A–4D). The dendritic ROIs are shown in the context of each neuron next to each map. The ubiquitination rate was measured for each condition. We observed a significant increase in the average ubiquitination rate in *Fmr1* KO neurons compared with the WT per unit area (Figures 4A, 4B, and 4E). Furthermore, we quantified the ubiquitination rate for WT and *Fmr1* KO neurons after treatment with Mdm2 inhibitor HLI373 or after vehicle. Mdm2 inhibition significantly reduced the elevated ubiquitination rate of PSD95 in *Fmr1* KO neurons but only had a trend to decrease this rate in WT neurons (Figure 4E). These results suggest that the observed aberrantly higher rate of PSD-95 ubiquitination in dendrites in *Fmr1* KO is Mdm2 dependent.

The above analysis of average rates of ubiquitination were done by imaging ubiquitination events in several dendritic ROIs that were at least 25 μm in length. To visualize the timing of appearance of new ubiquitination events within dendritic ROIs, Event *Schedules* (Figure 4F) were built by plotting the number of events detected over time in the dendrite segments shown in Figures 4A, 4B, 4C, and 4D. These event schedules show how the average rate is higher in *Fmr1* KO neurons compared with WT neurons, and how HLI 373 treatment determines a decrease in the ubiquitination rate in *Fmr1* KO neurons.

Our previous study using single-molecule detection of Venus-PSD-95 demonstrated an increased translation rate in *Fmr1* KO neurons, which correlated with a transient increase in steady-state levels of endogenous PSD-95 (Ifrim et al., 2015). Taken together with the present findings of increased PSD-95 ubiquitination in *Fmr1* KO, this suggests that the increased rate of PSD-95 ubiquitination in dendrites in *Fmr1*KO neurons may either

be compensatory to elevated translation and/or be attributed to increased PSD-95 levels. Comparison of ratios for PSD-95 translation (Ifrim et al., 2015) and ubiquitination rates in *Fmr1* KO neurons over WT neurons suggest a higher increase in translation over ubiquitination rate (Figure 4G). However, it is not possible to precisely determine from the comparison of these separate datasets if the increase in PSD-95 ubiquitination rate in *Fmr1*KO neurons matches or exceeds the rate increase expected to occur just due to the increase in translation and steady-state PSD-95 levels. Notably, the increased KO/WT PSD-95 ubiquitination rate was decreased by Mdm2 inhibitor HLI373 (Figure 4H). This suggests the effect of Mdm2 inhibition is more prominent in *Fmr1*KO neurons, which in turn would suggest that Mdm2-dependent PSD-95 ubiquitination is enhanced in *Fmr1* KO neurons.

Steady-state ubiquitination levels of PSD-95 are not changed in *Fmr1* KO neurons

To determine if the observed increase in the rate of PSD-95 ubiquitination in *Fmr1* KO neurons translates into increased steady-state levels of ubiquitinated PSD-95, we quantified PSD-95 steady-state ubiquitination in fixed cells using the Proximity Ligation Assay (PLA). To be able to directly compare the SM-UbFC experiments and PLA experiments, the ubiquitination levels of exogenously expressed PSD-95 should optimally be from a construct similar to the SM-UbFC construct. We transfected 14 DIV WT neurons with constructs expressing PSD-95 fused with full-length Venus (Ifrim et al., 2015) (Figure 5A, top). To ensure that we visualize only the ubiquitination of exogenously expressed PSD-95, for PLA we use antibodies against GFP (which recognize Venus) and antibodies against ubiquitinated proteins (FK2 clone). Thus, the PLA signal is generated only from the ubiquitinated Venus-PSD-95 WT construct.

To validate the method, technical and biological controls recommended were performed. Technical controls involved performing the PLA protocol without adding one or both antibodies. In all the conditions tested, omission of the antibody had the effect of dramatically reducing the PLA signal, suggesting the signal is specific for ubiquitinated Venus-PSD-95 (Figures 5B and 5C). The biological control involved the expression of PSD-95 containing mutations that replaced lysine residues known to be sites of ubiquitination (Bianchetta et al., 2011) (Figure 5A, bottom). This was the same PSD-95 lysine mutant used in SM-UbFC (Figures 2D–2F). PLA was performed after the expression of the Venus-PSD-95 Lys Mut and revealed a significant decrease in the PLA signal, consistent with decreased ubiquitination, as expected (Figures 5B and 5C). However, the degree of signal decrease was not as low as the technical controls, presumably because other ubiquitination sites are present in PSD-95 in addition to the ones removed. Indeed, a recent publication has identified additional ubiquitination sites in PSD-95 (Ma et al., 2017). Taken together, these results validate use of PLA analysis for determining the steady-state levels of total ubiquitination. PLA analysis of the steady-state levels of total ubiquitination of exogenous PSD-95 in 14DIV hippocampal neurons revealed no difference in *Fmr1* KO neurons compared with WT neurons (Figures 5D–5F).

Taken together with the finding of an increased PSD-95 ubiquitination rate and increased PSD-95 synthesis and steady-state levels in *Fmr1* KO neurons, the unchanged ubiquitination

steady-state levels could be attributed to increased PSD-95 degradation by the UPS system (the increased degradation by UPS would not be captured by looking at steady-state levels of ubiquitinated PSD-95), and possibly to a relative decrease in non-degradation related PSD-95 ubiquitination (discussion).

SM-UbFC reveals increased ubiquitination of GluA1 following GluR stimulation

Stimulation of mGluR receptors is known to induce LTD, which involves a decrease in the levels of surface AMPA receptors (Waung et al., 2008). AMPA receptor endocytosis entails ubiquitination of all AMPA subunits (Widagdo et al., 2015). The ubiquitination of GluA1 has been analyzed mostly biochemically, but has not been visualized directly in dendrites. We used SM-UbFC to directly visualize GluA1 ubiquitination in dendrites.

To test if SM-UbFC could detect fluctuations in the ubiquitination rate following a stimulation paradigm, we analyzed GluA1 ubiquitination in 14DIV neurons following mGluR stimulation. GluA1-specific UbFC constructs were generated (Figure 6A) and expressed in 14DIV hippocampal neurons (Figure 6B). Time-lapse imaging in live neurons was performed before and after addition of DHPG. Data were analyzed and Event maps were generated for equal time intervals before and after addition of DHPG. The number of events detected after DHPG was increased compared with before DHPG (Figures 6C and 6E). An event schedule was created to show the fluctuation of GluA1 ubiquitination before and after DHPG. After DHPG treatment, the GluA1 ubiquitination rate increased gradually, within a few minutes, to levels significantly higher than that observed before DHPG (Figure 6D). An increased rate of GluA1 ubiquitination was detected after 1 min. Ubiquitination of GluA1 was detected in dendrites. After vehicle treatment, the GluA1 ubiquitination rate did not change (Figure 6F).

SM-UbFC reveals increased ubiquitination of FMRP following GluR stimulation

FMRP is an RNA binding protein that has been shown to act as an inhibitor of translation for certain target mRNAs. The switch between the phosphorylated and un-phosphorylated forms of FMRP is coupled with translation inhibition and inhibition release, respectively (reviewed in Bassell and Warren [2008]). In addition to dephosphorylation, the inhibitory effect of FMRP is released also through FMRP ubiquitination and degradation (Bassell and Warren, 2008; Nalavadi et al., 2012). The ubiquitination of FMRP has been analyzed mostly biochemically, but has not been visualized directly in dendrites. In order to visualize directly FMRP ubiquitination in dendrites, FMRP-specific UbFC constructs were generated (Figure 7A) and expressed in 14 DIV hippocampal neurons.

The neurons were imaged by time-lapse microscopy before and after addition of DHPG. Data were analyzed as previously described and used to generate Event maps corresponding to equal time intervals before and after addition of DHPG. The number of events observed after DHPG addition was increased compared with before DHPG (Figures 7B–7D). An increased rate of FMRP ubiquitination in response to DHPG was detected after 1 min (Figure 7C). Ubiquitination of FMRP was detected in dendrites. After vehicle treatment, the FMRP ubiquitination rate did not change (Figure 7E).

DISCUSSION

Here we report development and application of a method, Single-Molecule Ubiquitin Mediated Fluorescence Complementation (SM-UbFC), for visualization and quantification of the spatiotemporal dynamics of ubiquitination in live cells. SM-UbFC can be used for visualizing *de novo* ubiquitination events in live cells and measurement of the global ubiquitination rate (compounded mono and polyubiquitination) with a high temporal, spatial, and molecular resolution, allowing for detection of the ubiquitination sites and is suitable for visualizing ubiquitination in dendrites. The length or the type of ubiquitin chain cannot be addressed using this method, which will measure just a global ubiquitination rate. Here we have adapted SM-UbFC to visualize the dynamics of protein ubiquitination in dendrites in response to plasticity-inducing stimuli. We apply this method to establish that PSD-95 is ubiquitinated in dendrites and demonstrate that PSD-95 ubiquitination rate is altered in a mouse model of FXS as evident by increased global PSD-95 ubiquitination rate. Herein we further show that GluA1 ubiquitination in dendrites is increased following the activation of mGluRs. These data are consistent with previous reports indicating that all subunits of AMPA receptors undergo ubiquitination prior to endocytosis (Widagdo et al., 2015). We further show that FMRP ubiquitination rate in dendrites increases following the activation of mGluRs. These data are consistent with previous studies showing that FMRP ubiquitination is activity regulated (Nalavadi et al., 2012; Huang et al., 2015; Hou et al., 2006).

FXS, caused by the inherited loss of the fragile X messenger ribonucleoprotein (FMRP), an mRNA binding protein, is the most common form of inherited intellectual disability and the leading monogenetic cause of autism. Several studies have shown, both by biochemistry and imaging, that the translation of FMRP target mRNAs is increased and dysregulated in FXS models. We have previously shown that PSD-95 synthesis is elevated and dysregulated in a model of FXS (Muddashetty et al., 2007, 2011; Ifrim et al., 2015). While the role of FMRP to regulate mRNA translation and protein synthesis in dendrites is now well established (Banerjee et al., 2018), emerging evidence suggests that FXS may be more broadly characterized by dysregulation of proteostasis in dendrites and spines. Studies on PSD-95 have served as a valuable model. PSD-95 is an abundant core component of the postsynaptic density that plays important roles in glutamate receptor trafficking, synaptic plasticity, and dendritic spine morphology (Bhattacharyya et al., 2009; De Roo et al., 2008; Xu et al., 2008). The synthesis and ubiquitination of PSD-95, an FMRP target, is dysregulated in FXS. PSD-95 ubiquitination is linked to MEF2-dependent synapse elimination and is altered in *Fmr1* KO neurons (Tsai et al., 2012). A limitation of past studies using biochemical methods to measure protein ubiquitination is lack of spatiotemporal controls. Here we have used SM-UbFC to demonstrate an increased global ubiquitination rate of PSD-95 in dendrites in an FXS mouse model. While part of this increase could be compensatory to increased PSD-95 levels in *Fmr1* KO neurons, the increased response to Mdm2 inhibition suggests a genuine alteration in PSD-95 ubiquitination in *Fmr1* KO neurons. This dysregulation of PSD-95 ubiquitination could impair synaptic localization or synaptic residence time of PSD-95 molecules. One model to test is whether PSD-95 synthesis, ubiquitination, and degradation rates may all be elevated, which would suggest a reduced half-life of newly

synthesize PSD-95. As dendritic spines are less stable in fragile X (Suresh and Dunaevsky, 2017; Cruz-Martin et al., 2010), it will be interesting in the future to assess a role for elevated rates of PSD-95 synthesis, ubiquitination, and turnover. *Future* studies might also address the dynamics of the PSD-95 carrying various types of ubiquitin chains in dendrites and spines.

Our findings that FMRP and GluA1 are also rapidly ubiquitinated in dendrites have implications for understanding mechanisms of mGluR-LTD. Several studies have shown that impairments in protein synthesis regulation in FXS lead to altered synaptic plasticity. LTD, which involves AMPA receptor endocytosis, is enhanced in response to activation of mGluRs in a mouse model of FXS (Huber et al., 2002). AMPA receptor endocytosis is preceded by ubiquitination of all AMPA receptor subunits (Widagdo et al., 2015). mGluR-dependent LTD is protein synthesis dependent in control neurons, but the enhanced LTD is protein synthesis independent in FXS (Nosyreva and Huber, 2006). Loss of FMRP in FXS may also result in impairments in the regulation of protein ubiquitination and there are interrelationships of E3 ligases with FMRP. The Mdm2 E3 ubiquitin ligase, which ubiquitinates PSD95, is necessary for mGluR activated translation (Liu et al., 2017). Surprisingly, FMRP was shown to be required for the ubiquitination and downregulation of Mdm2 (Liu et al., 2017). The Cdh1-APC E3 ligase was shown to directly ubiquitinate FMRP and be required for mGluR-LTD (Huang et al., 2015). More recently, we showed that Cdh1 also regulates FMRP associated proteins involved in stress granule assembly (Valdez-Sinon et al., 2020). Taken together, these studies underlie important links between protein synthesis and ubiquitination in synaptic plasticity, which are altered in FXS and other related neurodevelopmental brain disorders. Altered ubiquitination of several synaptic proteins, including PSD-95, has been reported in FXS models (Liu et al., 2017; Tsai et al., 2012), as analyzed using biochemical methods. A key question to be addressed is whether the ubiquitination levels and ubiquitination rates of other synaptic proteins within dendrites and dendritic spines are dysregulated in FXS. The present study using split-Venus fluorescent protein-based ubiquitination reporters, coupled with single-molecule imaging provides an approach to visualizing de *novo* ubiquitination in live cells with high spatial and temporal resolution and to address important questions relevant to synapse proteostasis in health and disease.

Limitations of the study

Our study makes use of SM-UbFC, which images the global ubiquitination rate of a protein of interest in live cells. SM-UbFC cannot, however, distinguish between mono- and polyubiquitination, between different types of polyubiquitin chains, or between different sites of ubiquitination on the protein of interest. SM-UbFC cannot, therefore, identify the consequences of an ubiquitination event, broadly it cannot distinguish if the ubiquitination event visualized has as consequence the targeting of the protein for degradation or just a change in functionality. Given the high complexity of the types of ubiquitination and the limitations of SM-UbFC in identifying them, the conclusions we can draw are limited and multiple lines of evidence by various methods are needed to constrain the interpretation possibilities regarding the SM-UbFC data.

Another limitation in this particular case is the fact that PSD-95 translation and steady-state levels are known to be increased in *Fmr1* KO neurons. While this increase in PSD-95 levels could not account for all the increase in the ubiquitination levels observed, it does nevertheless contribute to it. We speculate that increased ubiquitination may be compensatory to increased translation, leading to degradation and shorter half-life of newly synthesized proteins.

Another limitation of the method is that the complemented Venus molecule does not dissociate once formed, unlike ubiquitination dynamics that are reversible.

STAR★METHODS

RESOURCE AVAILABILITY

Lead contact—Further information and requests for resources and reagents should be directed to and will be fulfilled by the Lead Contact, Marius F. Ifrim (ifrimm@upstate.edu).

Materials availability—There are restrictions to the availability of the plasmids due to a requirement for an MTA prior to making them available.

Data and code availability

- This study did not generate any code.
- The datasets supporting the current study have not been deposited in a public repository because of the large size of single-molecule imaging raw data files, but are available from the corresponding author on request.
- The Octane plugin for ImageJ plugins used to analyze single-molecule imaging data was previously published (Tatavarty et al., 2012) and is available at: https://health.uconn.edu/yu-lab/software

EXPERIMENTAL MODEL AND SUBJECT DETAILS

Primary hippocampal neurons culture—Hippocampal neurons were isolated from male C57BL/6J- (WT) (IMSR Cat# JAX: 000664, RRID:IMSR_JAX: 000664) or B6.129P2-*Fmr1* ^{tm1Cgr}/J (*Fmr1*KO) (IMSR Cat# JAX: 003025, RRID:IMSR_JAX: 003025) E16.5 mouse embryos as previously described (Gao et al., 2008) and plated on 35 mm glass bottom culture dishes (MatTek) coated with poly-D-lysine (Sigma-Aldrich).

For all single-molecule imaging experiments, dishes were cleaned as previously described (Tatavarty et al., 2009, 2012). Briefly, dishes were sonicated 30 min in EtOH, 30 min in 10% NaOH, and 30 min in Milli-Q water (Millipore). The dishes were coated with 0.1 mg/mL poly-D-lysine (Sigma-Aldrich) in borate buffer, incubated overnight at 37°C, rinsed three times with Milli-Q water, and dried.

Neurons were maintained in neurobasal medium supplemented with 2% B27 (Thermo Scientific, Waltham, MA), and 1% Glutamax (Thermo Scientific, Waltham, MA), at 37°C and 5% CO2 for 13–15 days until transfection.

Cell lines—Neuro-2a (ECACC Cat# 89121404, RRID: CVCL_0470) male mouse neuroblastoma cells were used for proof of principle experiments due to the fact that they have a better transfection efficiency than hippocampal neurons. For single-molecule imaging experiments, dishes were cleaned as described for neurons. Neuro2A cells were plated at ~50% density and grown in 10% FBS DMEM for 1 day until transfection.

SY-SH5Y human neuroblastoma cell line (ATCC Cat# CRL-2266, RRID: CVCL_0019) (a gift from Jie Jiang) was used for the western blotting and immunoprecipitation experiments due to low endogenous PSD-95 expression. Cell cultures were plated at 40% density in 10 cm tissue culture dishes for immunoprecipitation or 12 well plates for the cell lysate western blotting assays and grown for 1 day in the same media as Neuro-2a cells until transfection.

METHOD DETAILS

Constructs—For Single-molecule ubiquitin mediated fluorescence complementation (SM-UbFC) experiments we used ubiquitin mediated fluorescence complementation (Hu et al., 2002; Fang and Kerppola, 2004) of Venus fluorescent protein (Nagai et al., 2002). Venus1-155 and Venus156-239 fragments were used (Shyu et al., 2006). We started with pUbFC-YN173Ub, pUbFC-YN173SUMO1 and pBiFC-JunCC155 plasmids, which were a gift from Dr. Thomas Kerpolla at Univ of Michigan, and substituted YFP fragments with Venus fragments: YN173 with Venus 1-155, and YC155 with Venus156-239. **BIFC-Ub WT (Venus-1-155-Ubiquitin)** plasmid was subcloned starting from the YFP-1-173 Ubiquitin plasmid. YFP1- 173 was excised between HinDIII and BglII restriction sites and replaced with Venus 1-155. **pBiFC-JunVenus-156-239** was subcloned from pBiFC-JunCC155 by inserting Ven156-239 between Asp78 and AauI restriction sites.

To increase the specificity of the fluorescence complementation between the two fragments of Venus, Valine 150 in Venus1-155 fragment was replaced with alanine, as previously described (Nakagawa et al., 2011), using the following primers: Forward: 5’- GGAGTACAACTACAACAGCCACAACGCCTATATCACCGCCGCG-3′: Reverse: 5’-CGCGGCGGTGATATAGGCGTTGTGGCTGTTGTAGTTGTACTCC-3′. **BIFC-Ub G76A (Venus-1-155-Ubiquitin with G76A mutation)**, which is ubiquitinated at a much lower rate and cannot be deubiquitinated (Hodgins and Ellison, 1992) was generated from **BIFC-Ub WT.** Gly76 was substituted with Alanine using QuickChange II XL Site-Directed Mutagenesis Kit (Agilent Technologies, La Jolla, CA) according to manufacturer’s instructions**. BIFC- ΔUbiq** (which lacks completely the ubiquitin ORF), was generated from **BIFC-Ub WT** by excising the ubiquitin between the two EcoRI restriction, followed by sticky end ligation of the plasmid ends. All constructs were confirmed by sequencing (Beckman Coulter, Brea, CA).

BiFC-PSD-95 WT (Venus (156-239)-PSD-95) plasmid, was subcloned from Venus-PSD-95 plasmid (Ifrim et al., 2015), by substituting Venus ORF for Venus-156-239 fragment between AgeI (BshTI) and NotI restriction sites. Venus-156-239 was PCR amplified using the following primers: Forward: 5’-GCTAGCGCTACCGGTCGCCACCATGGACAAGCAGAAGAACGGC-3′; Reverse:5′-GTC CAT GGC GGC CGC GCC GCT GCC GCC GCC GCT GCC GCC GCC GCT GCC

GCC GCC CTT GTA CAG CTC GTC C -3. BiFC-PSD-95 WT XXYX contains mouse PSD-95 5′UTR, ORF, 3′UTR and Venus (156-239), situated upstream of PSD-95 ORF.

BiFC-PSD-95 Lys Mut was generated by substituting PSD-95 lysines 10, 440, 543,672-679 with alanine residues. The primers used were: K10A mutation: Forward: 5’- GTCTCTGTATAGTGACAACCGCGAAATACCGCTACCAAGATG-3′; Reverse: 5’- CATCTTGGTAGCGGTATTTCGCGGTTGTCACTATACAGAGAC-3′. K403A mutation: Forward: 5’- GCCGATTCGAGGCCGCGATCCATGATCTTCGGG-3′; Reverse: 5’- CCCGAAGATCATGGATCGCGGCCTCGAATCGGC-3′. K544A mutation: Forward:5’- CCTTGGGCCTACCGCAGACCGTGCCAACG-3′; Reverse: 5’- CGTTGGCACGGTCTGCGGTAGGCCCAAGG-3′. K672A and K679A mutations: Forward: 5’- GCAAGCCCGGGCAGCCTTCGACAGGGCCACGGCGCTGGAGCAGG-3′; Reverse: 5’- CCTGCTCCAGCGCCGTGGCCCTGTCGAAGGCTGCCCGGGCTTGC-3′.

Venus-PSD-95 Lys Mut was subcloned from Venus-PSD-95 by replacing WT PSD-95 ORF with PSD-95 ORF with lysine mutations from **BiFC-PSD-95 Lys Mut** between NotI and SpeI restriction sites.

BIFC-GluA1**(BIFC-GluA1-Venus(156-239))** construct this construct was generated by replacing Jun ORF with GluA1 ORF in pBiFC-JunVenus-156-239 by Dr. Oskar Laur at Emory Custom Cloning Division Services.

BIFC-FMRP (Venus(156-239)-FMRP-3UTR) was subcloned from Venus-FMRP-3UTR (Suhl et al., 2015) by replacing Venus ORF with Venus(156-239) between AgeI and NotI restriction sites. The primers used to amplify Venus (156-239) were: Forward: 5’- CCGCTAGCGCTACCGGTCGCCACCATGGACAAGCAGAAGAACGGC-3′; Reverse: 5’- GCCGTTCTTCTGCTTGTCCATGGTGGCGACCGGTAGCGCTAGCGG-3′.

His-Venus vector was previously reported (Ifrim et al., 2015).

His-Venus purification and *in vitro* imaging were performed as reported previously (Ifrim et al., 2015).

pcDNA 3.1 (−) mammalian expression vector was acquired from Invitrogen. pmScarlet-i_C1 was a gift from Dorus Gadella (Addgene plasmid # 85044; http://n2t.net/addgene:85044; RRID:Addgene_85044).

Cell transfections—Neurons were transfected using CalPhos Mammalian Transfection Kit (Clontech Laboratories, Mountain View, CA) according to manufacturer’s instructions. After transfection, neurons were maintained for 20 h in neurobasal medium supplemented with 2% B27 (Thermo Scientific, Waltham, MA), and 1% Glutamax (Thermo Scientific, Waltham, MA), at 37°C and 5% CO_2. Just before starting the imaging, the neuro-basal medium was replaced with Hibernate E low fluorescence (Brain bits, Springfield, IL).

Neuro2A cells were transfected using Lipofectamine 2000 (Invitrogen, Carlsbad, California) according to manufacturer’s instructions. After transfection, Neuro2A cells were maintained for 20 h in 10% FBS DMEM at 37°C and 5% CO_2. Just before starting the imaging, the

10% FBS DMEM medium was replaced with Hibernate E low fluorescence (Brain bits, Springfield, IL).

SY-SH5Y cells were transfected with PEI MAX 40K (Avantor 75800-188, Polysciences Inc.), diluted in sterile dH_2O at 1 μg/mL. For immunoprecipitation, 12 μg of plasmid DNA and 36 μL of PEI were used per 10 cm dish. A separate mix of DNA and PEI was prepared (750 μL DMEM without serum each). Then DNA and PEI solutions were combined, incubated for 30 min in RT, and gently added to the cells. For the cell lysate western blotting assays, 2 μg of DNA, 3 μL of PEI, and 200 μL media total were used per well. Cells were transfected with BiFC-PSD-95 WT and BIFC-Ub WT or BIFC-Ub G76A at a 1:1 ratio. Controls were transfected with either BiFC-PSD-95 WT or BIFC-Ub WT and empty pcDNA 3.1 (−) plasmid vector. For the western blotting assays, cells were transfected with one of the vectors: BiFC-PSD-95 WT, BiFC-PSD-95 Lys Mut, BIFC-Ub WT or BIFC-Ub G76A, and pmScarlet-i_C1 as transfection control at 1:1 ratio. Following transfection, cells were maintained in the incubator overnight in the 10% FBS DMEM.

Single-molecule microscopy—Single-molecule imaging of ubiquitin mediated Venus complementation events was done as previously described for single-molecule imaging of translation using Venus fused constructs (Tatavarty et al., 2012; Barbarese et al., 2013; Ifrim et al., 2015). Single-molecule imaging was performed in wide field mode with a modified N-SIM microscope (Nikon, Tokyo, Japan), equipped with a 100X, NA = 1.49 microscope objective (Nikon, Tokyo, Japan) and an iXon3 EMCCD camera (Andor Technology USA, South Windsor, CT). For single molecule imaging of Ubiquitin-mediated fluorescence complementation in live cells (SM-UbFC), reconstituted Venus protein was excited with a 514 nm laser line (10mW), (Nikon, Tokyo, Japan). Following whole cell photobleaching, single-molecule time-lapse images of reconstituted Venus protein were collected continuously at an exposure time of 150 ms per frame. To minimize the effects of photo-damage on the cells an illumination area of ~15 μm diameter was used. Venus fluorescent protein is a fast folding variant of YFP (Nagai et al., 2002), which has bio-physical properties that make it suitable for single-molecule imaging (Yu et al., 2006). Venus has a fast folding of ~2 min *in vitro* and ~7 min in bacteria (Xie et al., 2008) making it suitable for imaging local fast molecular events, such as translation or ubiquitination, because the fast folding favors detection of Venus soon after translation or after split Venus complementation and, therefore, close to the site where the event took place. Venus also has fast-bleaching kinetics (Xie et al., 2008) allowing for the maintenance of a low fluorescence level in the cell necessary for the detection of individual newly folded Venus molecules.

In drug treatment experiments in which a significant time (15 or 30 min) was required for the drug effect, cells we incubated at 37°C for the required time with the drug and then the medium was replaced with HibE containing the drug at the same concentration. In contrast, in experiments where an acute (2–10 min) drug effect was investigated (DGPH treatment experiments), cells were imaged prior to and after the drug or vehicle were added.

Analysis of single-molecule images—Data analysis of time-lapse images was done as previously described (Yu et al., 2006; Tatavarty et al., 2012; Ifrim et al., 2015). Briefly, the centroid coordinates of individual molecules in each frame were determined and linked in

time to construct temporal trajectories, using a standard single-particle tracking algorithm. Each reconstituted Venus molecule detected was tracked from appearance (maturation) to disappearance (bleaching). For each molecule detected the centroid coordinates and timing of its first appearance were recorded. Preexisting reconstituted Venus fluorescent signal was used to manually define a region of interest that contained neuronal dendrites but not the cell body, for each dataset. From each dataset ubiquitination events situated inside the region of interest were analyzed with ImageJ (ImageJ, RRID: SCR_003070). The Octane plugin for ImageJ is available at https://health.uconn.edu/yu-lab/software. Event maps, to visualize the spatial distribution of ubiquitination events, and Event schedules, to visualize their temporal distribution, were created as previously described (Ifrim et al., 2015; Tatavarty et al., 2012).

Immunoprecipitation and western blotting: Cells were treated with 15 μM PR-619 (Tocris) for 20 min. Then, cells were scraped off in 500 ul of cold lysis buffer: (150 mM NaCl, 10 mM Tris-HCl, pH 7.5, 0.5 mM EDTA, 0.2% Triton X-) with protease inhibitor (cOmplete, EDTA-free Protease Inhibitor Cocktail, Roche) and 100 μM PR-619 (Tocris). Pierce Iodoacetamide, Single-Use (Thermo Scientific) was freshly diluted with the lysis buffer, then added to the extracts to the concentration of 10 mM. Then, extracts were kept on ice for 30 min, followed by centrifugation at 18,000 g for 30 min at 4°C. Supernatants were collected, then protein concentration was measured with a Pierce BCA Protein Assay Kit (Thermo Fisher Scientific). Aliquots were saved as Input fractions. The remaining supernatants (1.2 mg/sample) were added to 50 μL of GFP-Trap® Magnetic Particles M-270 (ChromoTek), washed beforehand twice in the lysis buffer, then incubated for 2.5 h at 4°C with rotation. Next, beads were washed once with lysis buffer, 3x with 8M Urea and 1% SDS in phosphate-buffered saline (PBS), and 1% SDS in PBS. Finally, samples were eluted by boiling the beads in 30 μL 2x Laemmli solution with 2-mercaptoethanol. Input fractions were boiled in 4x Laemmli solution with 2-mercaptoethanol. Half of each IP sample was loaded on the gel. As for Input fractions, 20 μg of total protein was used.

For the cell lysate western blotting assays, cells were harvested in 100 μL of the cold lysis buffer as above, then incubated on ice for 30 min and centrifuged at 18000 g for 30 min. Supernatants were collected, and protein concentration was measured with Pierce BCA Protein Assay Kit (Thermo Fisher Scientific). 20 μg of total protein per sample was loaded on a gel.

Western blotting was performed as follows: 4–20% Mini-PROTEAN® TGX™ Precast Protein Gels, 10-well (Bio-Rad) were run at 110 V until the dye reached the bottom of the gel. Then, proteins were transferred to the nitrocellulose membrane 0.2 μm (Bio-Rad) in a Mini Trans-Blot setup (Bio-Rad) at 110 V for 95 min at 4°C. Membranes were incubated in blocking buffer (5% non-fat dry milk in PBS with 0.01% Tween) for 1.5 h, then incubated in antibody diluted in blocking buffer overnight at 4°C with gentle rocking. Membranes were then washed 3 × 5 min in PBS with 0.01% Tween and incubated with secondary antibody diluted in blocking buffer for 1.5 h. After 3x wash with PBS with 0.01% Tween, blots with IP samples were developed with Tanon™ High-sig ECL Western Blotting Substrate (ABclonal). All other blots were incubated with fluorescent secondary antibodies (details in the STAR table). All membranes were imaged with a ChemiDoc imaging system (Bio-Rad).

Immunocytochemistry—For immunocytochemistry primary neurons in culture were washed twice with PBS (4°C), fixed in 4% paraformaldehyde for 20 min at room temperature, permeabilized with 0.1% Tergitol (Type NP40) (Sigma, St. Louis, MO) for 90 s and incubated for 1h in 10% horse serum in PBS for blocking. The samples were subsequently incubated with primary antibodies for 30 min [(1:500) in 10% horse serum,0.1% Triton X-100 PBS], followed by washing with PBS, 3 times, 5 min each, and incubation with secondary antibodies[(1:500) in 10% horse serum,0.1% Triton X-100 PBS], followed by washing with PBS, 3 times, 5 min each,. Finally the sample were mounted with ProLong™ Diamond Antifade Mountant (Thermo Scientific, Rockford, Il).

The antibodies used were:

Primary Antibodies used were: Anti GFP (chicken), (Aves Labs Cat# GFP-1010, RRID:AB_2307313), (Aves Labs, Tigard, OR); Anti-20S Proteasome Core Subunits Rabbit pAb, (Millipore Cat# ST1053-100UL, RRID:AB_437908), (Milipore, Billerica, MA).

Secondary antibodies used were: Alexa Fluor® 488 AffiniPure Donkey Anti-Chicken IgY (IgG) (H + L), (Jackson ImmunoResearch Labs Cat# 703-545-155, RRID:AB_2340375), (Jackson ImmunoResearch Laboratories, West Grove, PA) and Donkey anti-Rabbit, Alexa 546 conjugate, (Thermo Fisher Scientific Cat# A10040, RRID:AB_2534016), (Thermo Scientific, Waltham, MA).

Immunocytochemistry images were collected with a Nikon Eclipse epifluorescence microscope (Nikon, Tokyo, Japan) equipped with a 40X oil objective.

Proximity ligation assay (PLA)—Proximity ligation assay was performed using Duolink In Situ Red Starter Kit Mouse/Rabbit (Millipore Sigma, St. Louis, MO) according to manufactures instructions. 14DIV WT or *Fmr1*KO neurons were firstly transfected with either Venus-PSD-95 WT or Venus-PSD-95 Lys Mut. PLA was performed using the following pair of antibodies:

Anti-GFP antibody (ab6556), rabbit polyclonal, (Abcam Cat# ab6556, RRID: AB_305564) (Abcam, Cambridge, United Kingdom); Anti-Ubiquitinylated proteins Antibody, clone FK2, (Millipore Cat# 04-263, RRID:AB_612093), (Milipore, Billerica, MA).

PLA-imaging and analysis—PLA images were collected with a Nikon Eclipse epifluorescence microscope (Nikon, Tokyo, Japan), Equipped with a 40X oil objective. Separate channels were collected for Venus fluorescence and for the red fluorescence of the PLA signal.

In the red channel a threshold was used create binary images in which only the PLA puncta (corresponding to ubiquitinated PSD-95) are visible. Cell bodies and areas with high extracellular noise were excluded from analysis. ImageJ was used to automatically quantify the total number of PLA puncta in the dendrites of a neuron.

ImageJ was used to quantify the total length of the dendrites of each neuron. From the total number of PLA puncta and the total dendrite length was computed the number of PLA puncta per 10μm.

Drug treatments—S-DHPG (Tocris, Mineapolis, MN) was used at 50 μM to activate mGluR in neurons.

MG132 (Tocris, Mineapolis, MN), a preoteasome inhibitor was used at concentration of 10 uM.

HLI373 (Sigma, St. Louis, MO), a Hdm2 E3 Ligase Inhibitor was used at a concentration of 5μM (Kitagaki et al., 2008).

QUANTIFICATION AND STATISTICAL ANALYSIS

Each experiment was replicated at least three independent times. Normal distribution within all datasets was assessed using the Shapiro-Wilk's test. Datasets that showed normal distribution were analyzed with Student's t-test, general linear model (repeated measurements) or ANOVA (one-way, two-way). Datasets that did not display normal distribution were analyzed by the non-parametric Mann-Whitney or Kruskal-Wallis. The statistical test used specifically to analyze each experiment is given in the corresponding figure legend. Significance threshold was set as $p \leq 0.05$. All datasets are displayed as mean ± SEM. All datasets were analyzed using SPSS (IBM, Armonk, NY).

ACKNOWLEDGMENTS

We acknowledge support from the NIH: RO1MH109026 and 1R21NS091038 (to G.J.B.). This research was also supported in part by the Emory University Integrated Cellular Imaging Microscopy Core of the Emory Neuroscience NINDS Core Facilities grant, P30NS055077. We thank Dr. Ji Yu for providing the software used to analyze single-molecule data. We thank Dr. Oskar Laur and Emory Custom Cloning Core for cloning some of the plasmids used.

INCLUSION AND DIVERSITY

We support inclusive, diverse, and equitable conduct of research.

REFERENCES

Banerjee A, Ifrim MF, Valdez AN, Raj N, and Bassell GJ (2018). Aberrant RNA translation in fragile X syndrome: From FMRP mechanisms to emerging therapeutic strategies. Brain Res 1693, 24–36. [PubMed: 29653083]

Barbarese E, Ifrim MF, Hsieh L, Guo C, Tatavarty V, Maggipinto MJ, Korza G, Tutolo JW, Giampetruzzi A, Le H, et al. (2013). Conditional knockout of tumor overexpressed gene in mouse neurons affects RNA granule assembly, granule translation, LTP and short term habituation. PLoS One 8, e69989. [PubMed: 23936366]

Bassell GJ, and Warren ST (2008). Fragile X syndrome: loss of local mRNA regulation alters synaptic development and function. Neuron 60, 201–214. [PubMed: 18957214]

Bhattacharyya S, Biou V, Xu W, Schlüter O, and Malenka RC (2009). A critical role for PSD-95/AKAP interactions in endocytosis of synaptic AMPA receptors. Nat. Neurosci. 12, 172–181. [PubMed: 19169250]

Bianchetta MJ, Lam TT, Jones SN, and Morabito MA (2011). Cyclin-dependent kinase 5 regulates PSD-95 ubiquitination in neurons. J. Neurosci. 31, 12029–12035. [PubMed: 21849563]

Bingol B, and Schuman EM (2006). Activity-dependent dynamics and sequestration of proteasomes in dendritic spines. Nature 441, 1144–1148. [PubMed: 16810255]

Colledge M, Snyder EM, Crozier RA, Soderling JA, Jin Y, Langeberg LK, Lu H, Bear MF, and Scott JD (2003). Ubiquitination regulates PSD-95 degradation and AMPA receptor surface expression. Neuron 40, 595–607. [PubMed: 14642282]

Croucher D, Iconomou M, Hastings J, Kennedy S, Han JZR, Shearer R, Mckenna J, Wan A, Lau J, Aparicio S, and Saunders D (2016). Bimolecular complementation affinity purification (BiCAP) reveals dimer-specific protein interactions for ERBB2 dimers. Sci. Signal. 9, ra69. [PubMed: 27405979]

Cruz-Martín A, Crespo M, and Portera-Cailliau C (2010). Delayed stabilization of dendritic spines in fragile X mice. J. Neurosci. 30, 7793–7803. [PubMed: 20534828]

De Roo M, Klauser P, Mendez P, Poglia L, and Muller D (2008). Activity-dependent PSD formation and stabilization of newly formed spines in hippocampal slice cultures. Cereb. Cortex 18, 151–161. [PubMed: 17517683]

Ehlers MD (2003). Activity level controls postsynaptic composition and signaling via the ubiquitin-proteasome system. Nat. Neurosci. 6, 231–242. [PubMed: 12577062]

Fang D, and Kerppola TK (2004). Ubiquitin-mediated fluorescence complementation reveals that Jun ubiquitinated by Itch/AIP4 is localized to lysosomes. Proc. Natl. Acad. Sci. USA 101, 14782–14787. [PubMed: 15469925]

Gao Y, Tatavarty V, Korza G, Levin MK, and Carson JH (2008). Multiplexed dendritic targeting of alpha calcium calmodulin-dependent protein kinase II, neurogranin, and activity-regulated cytoskeleton-associated protein RNAs by the A2 pathway. Mol Biol Cell 19. 2311–27. [PubMed: 18305102]

Hodgins RR, and Ellison MJ (1992). Expression of a ubiquitin derivative that conjugates to protein irreversibly produces phenotypes consistent with a ubiquitin deficiency. J Biol Chem 267. 8807–12. [PubMed: 1315740]

Hou L, Antion MD, Hu D, Spencer CM, Paylor R, and Klann E (2006). Dynamic translational and proteasomal regulation of fragile X mental retardation protein controls mGluR-dependent long-term depression. Neuron 51, 441–454. [PubMed: 16908410]

Hu CD, Chinenov Y, and Kerppola TK (2002). Visualization of interactions among bZIP and Rel family proteins in living cells using bimolecular fluorescence complementation. Mol. Cell 9, 789–798. [PubMed: 11983170]

Huang J, Ikeuchi Y, Malumbres M, and Bonni A (2015). A Cdh1-APC/FMRP ubiquitin signaling link drives mGluR-dependent synaptic plasticity in the mammalian brain. Neuron 86, 726–739. [PubMed: 25913861]

Huber KM, Gallagher SM, Warren ST, and Bear MF (2002). Altered synaptic plasticity in a mouse model of fragile X mental retardation. Proc. Natl. Acad. Sci. USA 99, 7746–7750. [PubMed: 12032354]

Ifrim MF, Williams KR, and Bassell GJ (2015). Single-molecule imaging of PSD-95 mRNA translation in dendrites and its dysregulation in a mouse model of fragile X syndrome. J. Neurosci. 35, 7116–7130. [PubMed: 25948262]

Kim MJ, Futai K, Jo J, Hayashi Y, Cho K, and Sheng M (2007). Synaptic accumulation of PSD-95 and synaptic function regulated by phosphorylation of serine-295 of PSD-95. Neuron 56, 488–502. [PubMed: 17988632]

Kitagaki J, Agama KK, Pommier Y, Yang Y, and Weissman AM (2008). Targeting tumor cells expressing p53 with a water-soluble inhibitor of Hdm2. Mol. Cancer Ther. 7, 2445–2454. [PubMed: 18723490]

Lin AW, and Man HY (2013). Ubiquitination of neurotransmitter receptors and postsynaptic scaffolding proteins. Neural Plast. 2013, 432057. [PubMed: 23431475]

Liu DC, Seimetz J, Lee KY, Kalsotra A, Chung HJ, Lu H, and Tsai NP (2017). Mdm2 mediates FMRP- and Gp1 mGluR-dependent protein translation and neural network activity. Hum. Mol. Genet. 26, 3895–3908. [PubMed: 29016848]

Ma Q, Ruan H, Peng L, Zhang M, Gack MU, and Yao WD (2017). Proteasome-independent polyubiquitin linkage regulates synapse scaffolding, efficacy, and plasticity. Proc. Natl. Acad. Sci. USA 114, E8760–E8769. [PubMed: 28973854]

Muddashetty RS, Kelic S, Gross C, Xu M, and Bassell GJ (2007). Dysregulated metabotropic glutamate receptor-dependent translation of AMPA receptor and postsynaptic density-95 mRNAs at synapses in a mouse model of fragile X syndrome. J Neurosci 27. 5338–48. [PubMed: 17507556]

Muddashetty RS, Nalavadi VC, Gross C, Yao X, Xing L, Laur O, Warren ST, and Bassell GJ (2011). Reversible inhibition of PSD-95 mRNA translation by miR-125a, FMRP phosphorylation, and mGluR signaling. Mol Cell 42. 673–88. [PubMed: 21658607]

Nagai T, Ibata K, Park ES, Kubota M, Mikoshiba K, and Miyawaki A (2002). A variant of yellow fluorescent protein with fast and efficient maturation for cell-biological applications. Nat. Biotechnol. 20, 87–90. [PubMed: 11753368]

Nakagawa C, Inahata K, Nishimura S, and Sugimoto K (2011). Improvement of a Venus-based bimolecular fluorescence complementation assay to visualize bFos-bJun interaction in living cells. Biosci Biotechnol Biochem 75. 1399–401. [PubMed: 21737916]

Nalavadi VC, Muddashetty RS, Gross C, and Bassell GJ (2012). Dephosphorylation-induced ubiquitination and degradation of FMRP in dendrites: a role in immediate early mGluR-stimulated translation. J. Neurosci. 32, 2582–2587. [PubMed: 22357842]

Nosyreva ED, and Huber KM (2006). Metabotropic receptor-dependent long-term depression persists in the absence of protein synthesis in the mouse model of fragile X syndrome. J. Neurophysiol. 95, 3291–3295. [PubMed: 16452252]

Patrick GN, Bingol B, Weld HA, and Schuman EM (2003). Ubiquitin-mediated proteasome activity is required for agonist-induced endocytosis of GluRs. Curr. Biol. 13, 2073–2081. [PubMed: 14653997]

Pickart CM, Kasperek EM, Beal R, and Kim A (1994). Substrate properties of site-specific mutant ubiquitin protein (G76A) reveal unexpected mechanistic features of ubiquitin-activating enzyme (E1). J. Biol. Chem. 269, 7115–7123. [PubMed: 8125920]

Schneider CA, Rasband, and Eliceiri KW (2012). NIH Image to ImageJ: 25 years of image analysis. Nat Methods 9. 671–5. [PubMed: 22930834]

Shyu YJ, Liu H, Deng X, and Hu CD (2006). Identification of new fluorescent protein fragments for bimolecular fluorescence complementation analysis under physiological conditions. Biotechniques 40, 61–66. [PubMed: 16454041]

Steward O, and Schuman EM (2003). Compartmentalized synthesis and degradation of proteins in neurons. Neuron 40, 347–359. [PubMed: 14556713]

Suhl JA, Muddashetty RS, Anderson BR, Ifrim MF, Visootsak J, Bassell GJ, and Warren ST (2015). A3' untranslated region variant in FMR1 eliminates neuronal activity-dependent translation of FMRP by disrupting binding of the RNA-binding protein HuR. Proc. Natl. Acad. Sci. USA 112, E6553–E6561. [PubMed: 26554012]

Suresh A, and Dunaevsky A (2017). Relationship between synaptic AMPAR and spine dynamics: impairments in the FXS mouse. Cereb. Cortex 27, 4244–4256. [PubMed: 28541473]

Tai HC, and Schuman EM (2008). Ubiquitin, the proteasome and protein degradation in neuronal function and dysfunction. Nat. Rev. Neurosci. 9, 826–838. [PubMed: 18931696]

Tatavarty V, Ifrim MF, Levin M, Korza G, Barbarese E, Yu J, and Carson JH (2012). Single-molecule imaging of translational output from individual RNA granules in neurons. Mol. Biol. Cell 23, 918–929. [PubMed: 22219377]

Tatavarty V, Kim EJ, Rodionov V, and Yu J (2009). Investigating subspine actin dynamics in rat hippocampal neurons with super-resolution optical imaging. PLoS One 4, e7724. [PubMed: 19898630]

Tsai NP, Wilkerson JR, Guo W, Maksimova MA, Demartino GN, Cowan CW, and Huber KM (2012). Multiple autism-linked genes mediate synapse elimination via proteasomal degradation of a synaptic scaffold PSD-95. Cell 151, 1581–1594. [PubMed: 23260144]

Valdez-Sinon AN, Lai A, Shi L, Lancaster CL, Gokhale A, Faundez V, and Bassell GJ (2020). Cdh1-APC Regulates Protein Synthesis and Stress Granules in Neurons through an FMRP-Dependent Mechanism. iScience 23, 101132. [PubMed: 32434143]

Waung MW, Pfeiffer BE, Nosyreva ED, Ronesi JA, and Huber KM (2008). Rapid translation of Arc/Arg3.1 selectively mediates mGluR-dependent LTD through persistent increases in AMPAR endocytosis rate. Neuron 59, 84–97. [PubMed: 18614031]

Widagdo J, Chai YJ, Ridder MC, Chau YQ, Johnson RC, Sah P, Huganir RL, and Anggono V (2015). Activity-dependent ubiquitination of GluA1 and GluA2 regulates AMPA receptor intracellular sorting and degradation. Cell Rep. 10, 783–795. [PubMed: 25660027]

Xie XS, Choi PJ, Li GW, Lee NK, and Lia G (2008). Single-molecule approach to molecular biology in living bacterial cells. Annu. Rev. Biophys. 37, 417–444. [PubMed: 18573089]

Xu W, Schlüter OM, Steiner P, Czervionke BL, Sabatini B, and Malenka RC (2008). Molecular dissociation of the role of PSD-95 in regulating synaptic strength and LTD. Neuron 57, 248–262. [PubMed: 18215622]

Yu J, Xiao J, Ren X, Lao K, and Xie XS (2006). Probing gene expression in live cells, one protein molecule at a time. Science 311, 1600–1603. [PubMed: 16543458]

Highlights

- Single-molecule imaging of *de novo* ubiquitination events in live cells
- FMR1 KO neurons display increased ubiquitination rate of PSD-95
- GluA1 global ubiquitination rate in dendrites increases after activation of mGluRs
- FMRP global ubiquitination rate in dendrites increases after activation of mGluRs

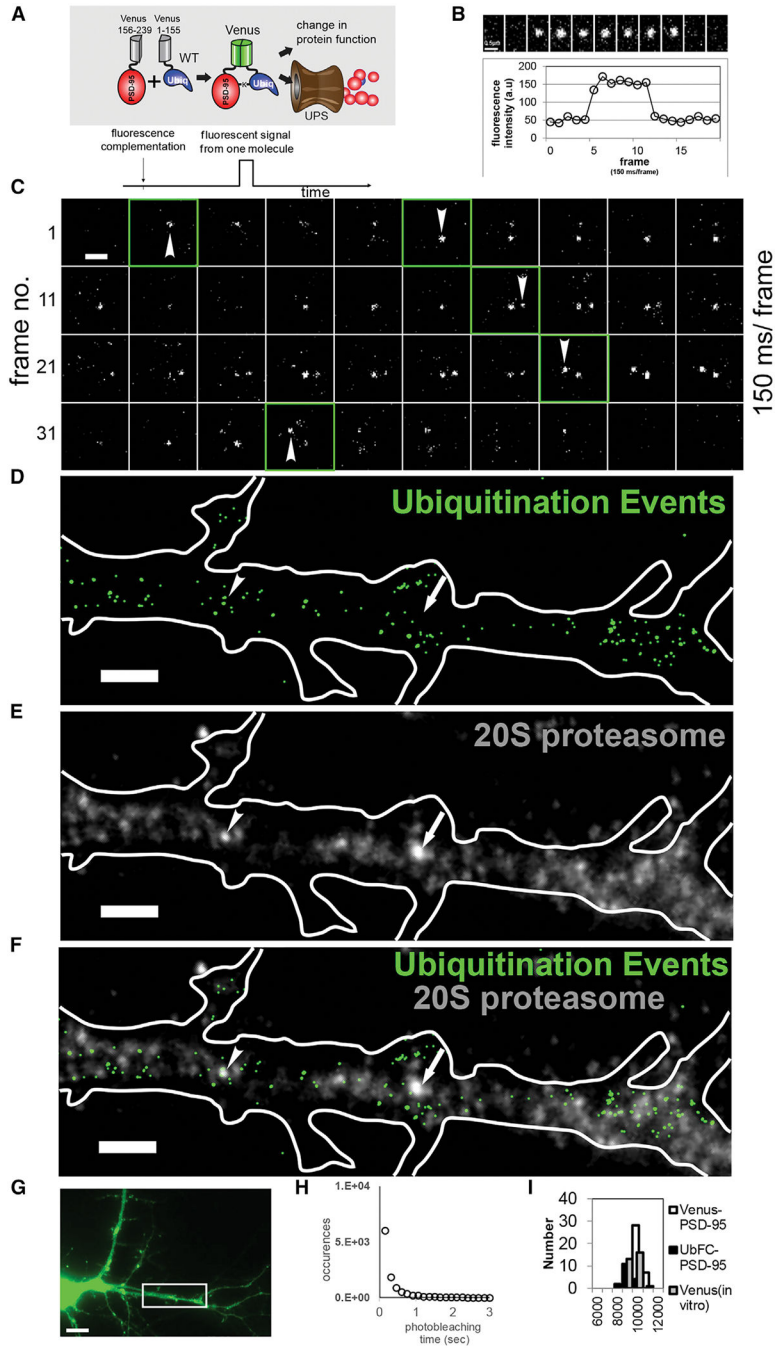

Figure 1. Visualization of *de novo* ubiquitination events in live neurons with high spatial and temporal resolution using SM-UbFC

(A) Diagram illustrating the bimolecular fluorescence complementation (BiFC) constructs for PSD-95 and ubiquitin fused to one of the halves of Venus: SM-UbFC principle; upon reconstitution of Venus, fast folding of Venus promotes its fast detection with single-molecule resolution. Fast bleaching of Venus promotes a low fluorescence background, permitting the detection of other reconstituted Venus molecules.

(B) Raw data montage showing one reconstituted split-Venus molecule detected. The quantification of fluorescence intensity over time indicates one-step appearance and one-step disappearance, which are characteristic for single-molecule imaging.
(C) Raw data montage showing appearance (arrows) and disappearance of flashes of light corresponding to fluorescent reconstituted Venus in live cells; molecules show one-step appearance and disappearance. Scale bar, 1 μm.
(D–F) Ubiquitination events are detected in a dendrite of a 14 DIV mouse hippocampal neuron. (D) Event map indicating the summary of positions of the ubiquitination events in the dendrite. (E) Immunocytochemistry for 20S proteasome. (F) Overlay. Scale bar, 2 μm.
(G) Fluorescent image of the whole neuron, the dendrite of which is shown in (D–F). The white box indicates the region of interest (ROI) shown in (D–F). Scale bar,10 μm.
(H) The bleaching kinetics of the particle detected by SM-UbFC in live cells were identical to those reported for Venus, with most of the molecule being bleached after 1 s of illumination. n > 10 K particles, from 11 cells derived from four different cell cultures.
(I) The distribution of the fluorescence intensity of the particles detected when UbFC constructs were used overlaps the distribution of fluorescence intensity of intact full-length Venus both *in vitro* and in live cells. n = 46/43/34 particles, for Venus-PSD-95 (one cell), UbFC-PSD-95 (two cells), Venus *in vitro* (one experiment), respectively.

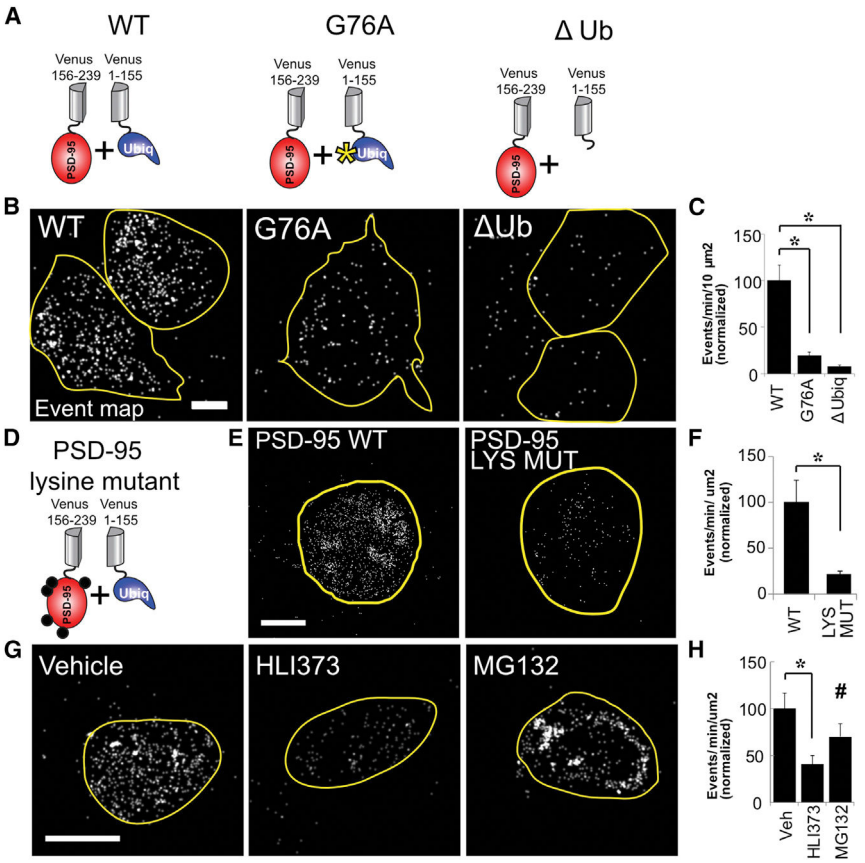

Figure 2. SM-UbFC signal shows specificity in live cells, as it decreases when the binding of ubiquitin to its target is perturbed, or when the specific E3 ligase is inhibited

(A) Diagrams for the WT and control constructs (G76A mutant and ubiquitin deletion (ΔUb).

(B) Representative ubiquitination event maps for WT, G76A mutant, and ubiquitin deletion (ΔUb) constructs. Scale bar, 5 µm.

(C) Representative experiment in N2A cells showing loss of Venus signal when G76A mutation is present or when ubiquitin is deleted (one-way ANOVA, $F(2, 15) = 29.63$, $p = 0.00$, Tukey HSD *post hoc* comparisons of G76A mutant and ubiquitin deletion to the WT *p(G76A) = 0.000, *p(ΔUb) = 0.000). $n \geq 16$ cells per condition, from three independent cultures, at least five cells per culture per condition.

(D) Diagram of the BiFC-PSD-95 Lys Mut construct, in which previously identified lysines known to be ubiquitinated were replaced with alanine. (E) Representative ubiquitination event maps for BiFC-PSD-95 WT (left) and BiFC-PSD-95 Lys Mut (right). Scale bar, 5 µm.

(F) Representative experiment showing loss of Venus signal when previously identified lysines in PSD-95 were replaced. *$p < 0.05$, Student test, $n \geq 20$ cells per condition from three independent cultures, at least five cells per culture per condition.

(G) Representative ubiquitination event maps for cells treated with vehicle, HLI373, or MG132 (as indicated). Scale bar, 5 µm.

(H) Cell treatment with HLI373, an Mdm2 inhibitor, leads to a significant decrease of the detected ubiquitination rate. Treatment with MG132 (a proteasome inhibitor) did not produce significant changes in the ubiquitination rate, while presenting with a trend decr)ase

in ubiquitination rate (one-way ANOVA, $F(2,43) = 5.49$, $p = 0.008$, Tukey HSD *post hoc* comparisons of HLI373 and MG132 treatments to the vehicle). $n \geq 13$ cells per condition, from three independent cultures, at least three cells per culture per condition. Data are represented as means ± SEM. *$p < 0.05$, # non-significant.

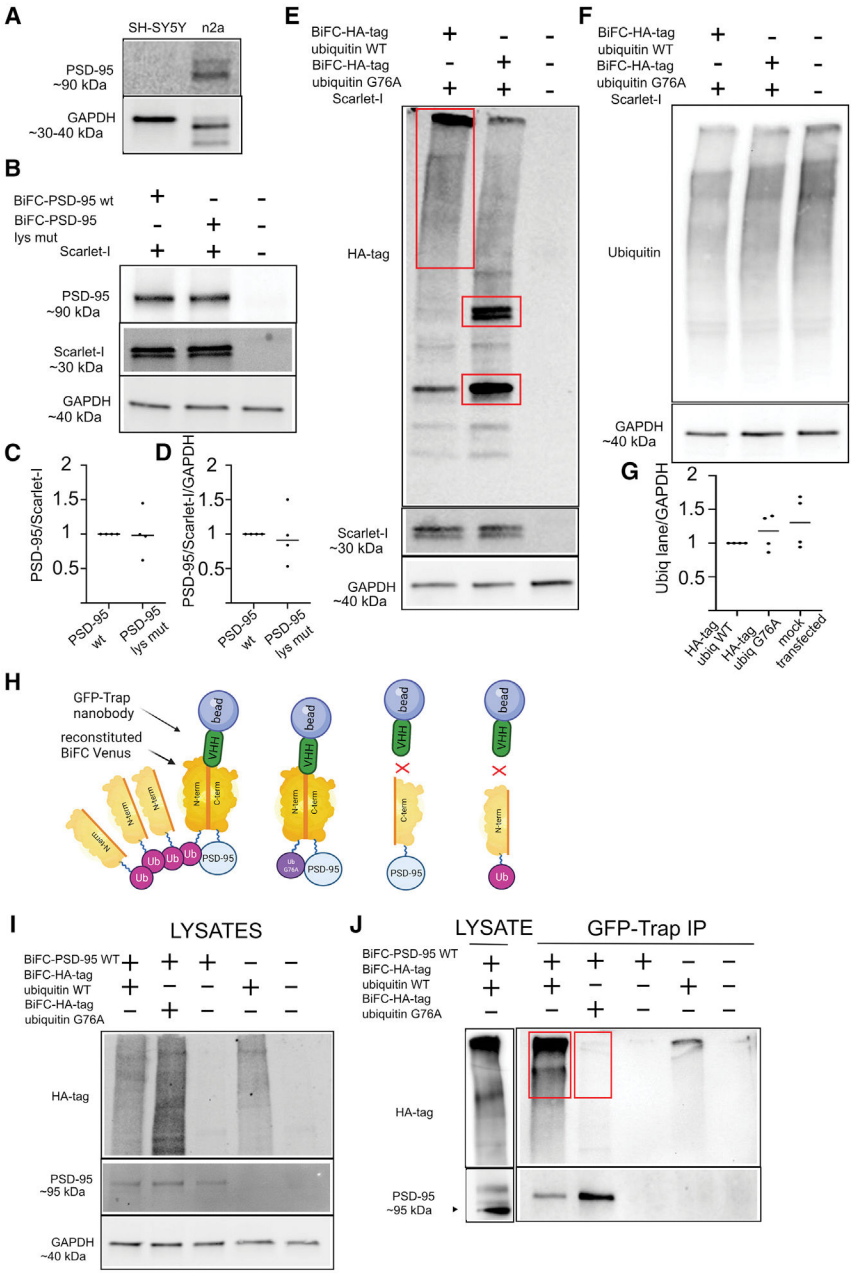

Figure 3. Expression controls for non-complemented BiFC-PSD-95 and BiFC-HA-Ubiquitin constructs

(A) Non-transfected SH-SY5Y or n2a cells were lysed, then endogenous PSD-95 levels were evaluated by western blot. SH-SY5Y exhibit very low endogenous PSD-95 when compared with n2a cells.

(B–D) SH-SY5Y cells were transfected with plasmids expressing either BiFC-PSD-95 WT or BiFC-PSD-95 Lys Mut and Scarlet-I for transfection control, then blots were probed for PSD-95, Scarlet-I or GAPDH. Expression levels of overexpressed BiFC-PSD-95 WT and BiFC-PSD-95 Lys Mut do not differ. (C) Mean intensity of PSD-95 normalized to Scarlet-I and then to the PSD-95 WT. One-sample t test, n = 4, ns, p = 0.9572. (D) Mean intensity of

PSD-95, normalized to Scarlet-I, then to GAPDH, then to the PSD-95 WT band as a control. One-sample t test, n = 4, ns, p = 0.8736.

(E) SH-SY5Y cells were transfected with plasmids expressing either BiFC-Ub WT or BiFC-Ub G76A mutant and Scarlet-I, then analyzed by the western blot probed for HA-tag, Scarlet-I, and GAPDH. Representative blot shows high molecular weight ubiquitinated protein species in the BiFC-Ub WT lane (large red box). BiFC-Ub G76A shows less high molecular weight ubiquitinated protein species and bands that may correspond to self-polymerized ubiquitin (Hodgins, Ellison and Ellison, 1992; red boxes).

(F and G) The same lysates were analyzed by the western blot probed for ubiquitin and GAPDH. €(E) and (F) show corresponding blots of the samples from the same experiment. Overexpression of BiFC-Ub WT or BiFC-Ub G76A mutant does not significantly affect total ubiquitinated protein levels. Intensity of the whole ubiquitin lane was normalized to GAPDH and to overexpressed BiFC-Ub WT lane (one-way ANOVA, F (2,9) = 1,308, p = 0.317, n = 4, ns).

(H) Biochemical confirmation of bimolecular fluorescence ubiquitin complementation of BiFC-PSD-95 WT with BiFC-Ub WT (BiFC-HA-Ubiquitin WT) using GFP-Trap pull down. Schematic of the method. GFP-Trap nanobody bound to magnetic beads pulls down BiFC Venus protein reconstituted due to formation of the PSD-95-polyubiquitin complex. G76A ubiquitin mutant protein binds PSD-95 less efficiently. Neither BiFC-PSD95 WT nor BiFC-Ub WT alone are pulled down by the GFP-Trap nanobody.

(I) Western blots on lysates prior to GFP-Trap. SH-SY5Y cells were transfected with plasmids expressing BiFC-PSD95 WT and either BiFC-Ub WT or BiFC-Ub G76A. Representative western blot of lysates used for the pull-down experiment, probed for HA-tag, PSD-95, and GAPDH.

(J) Western blot for HA-tag following GFP-Trap pull down show high molecular species complexes present in the PSD-95/Ubiq WT lane but not in the PSD-95/Ubiq G76A lane (red boxes). Western blot for PSD-95 shows a positive band that is stronger in the G76A Ubiq mutant and runs higher than the BiFC-PSD95 in the lysate. GFP-Trap pull down on single plasmid-transfected and control non-transfected cell lysates yields negative results. The last lane shows lysate co-transfected with BiFC-PSD-95 and BiFC-HA-Ubiquitin that was run on the same blot probed with anti-HA and anti-PSD-95 antibody respectively. The image was less saturated than the rest of the blot for visibility. (I) and (J) show lysates and corresponding IPs from the same experiment, and the lysate sample in (J) is the same as the first lysate in (I).

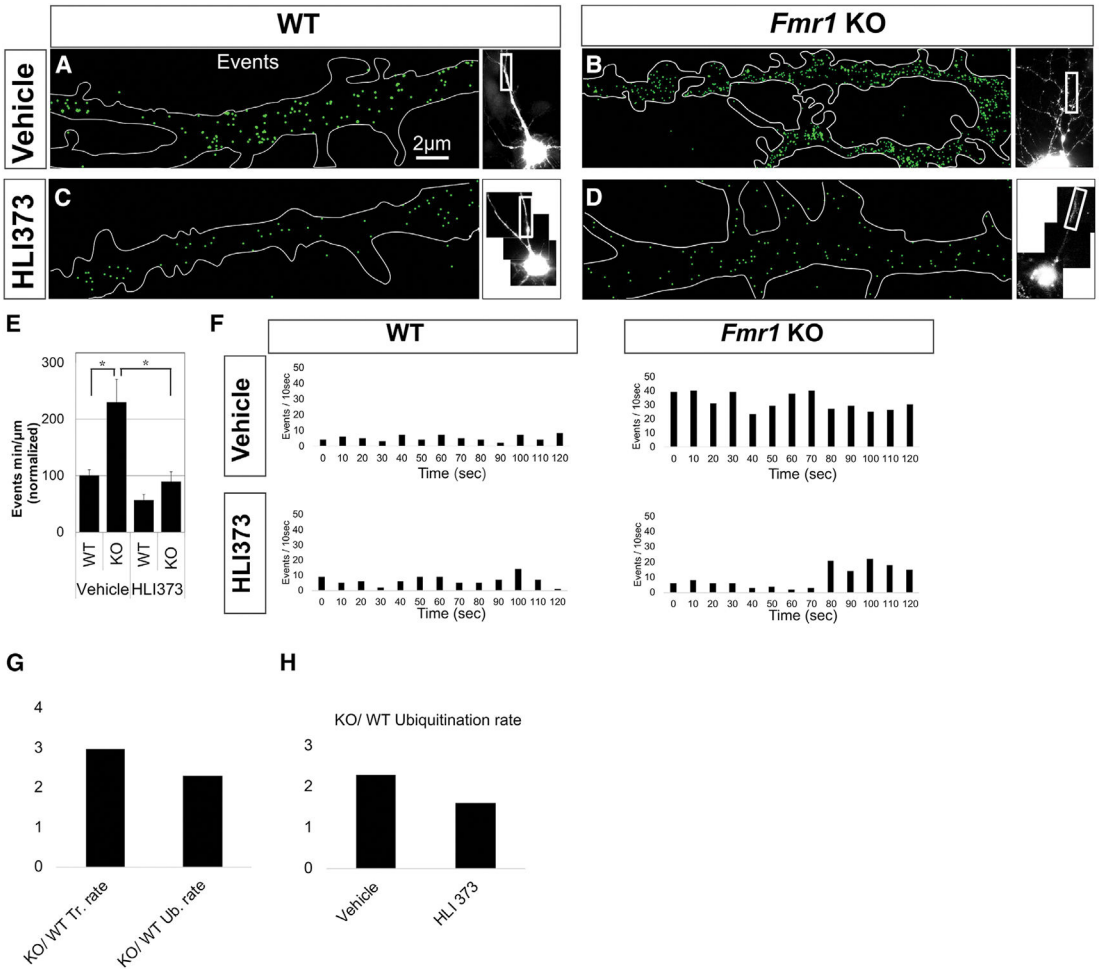

Figure 4. Increased ubiquitination rate of PSD-95 in dendrites *Fmr1* KO hippocampal neurons detected using SM-UbFC

(A–D) Event maps indicating the position of detected PSD-95 ubiquitination events in dendrites of representative 14DIV hippocampal neurons. Each green dot represents a ubiquitination event. The maps represent the ubiquitination events detected over a 2-min interval. (A) Event map of a dendrite segment of a representative 14DIV WT hippocampal neuron, treated with vehicle. (B) Event map of a dendrite segment of a representative 14DIV *Fmr1* KO hippocampal neuron, treated with vehicle. (C) Event map of a dendrite segment of a representative 14DIV WT hippocampal neuron, treated with Mdm2 inhibitor HLI 373. (D) Event map of a dendrite segment of a representative 14DIV *Fmr1* KO hippocampal neuron, treated with HLI 373. At the right of each event map there is a fluorescent image of the whole neuron. The white box indicates the ROI shown in the Event panel. Scale bar, 2 μm. (E) Quantification of the total ubiquitination rate in WT and *Fmr1* KO hippocampal neurons after vehicle or Mdm2 inhibitor HLI373 was added. *Fmr1* KO neurons showed a significantly increased effect of Mdm2 inhibitor compared with WT neurons (*-two-way ANOVA, genotype and treatment as fixed factors, genotype $F(1,64) = 13.2$, $p = 0.001$; treatment $F(1,64) = 16.85$, $p = 0.000$, interaction $F(1,64) = 4.63$, $p = 0.035$; For each condition $n = 15$, with at least three different cultures with at least three cells per culture. Data are represented as means ± SEM. *$p < 0.05$.

(F) Event schedules corresponding to WT neurons (left panels), or *Fmr1*KO neuron (right panels), treated with vehicle (top panels) or HLI 373 (bottom panels).
(G) KO/WT translation rate ratio (from Ifrim et al., 2015) versus KO/WT ubiquitination rate ratio. (H) KO/WT ubiquitination rate ratio following vehicle or HLI373 treatment.

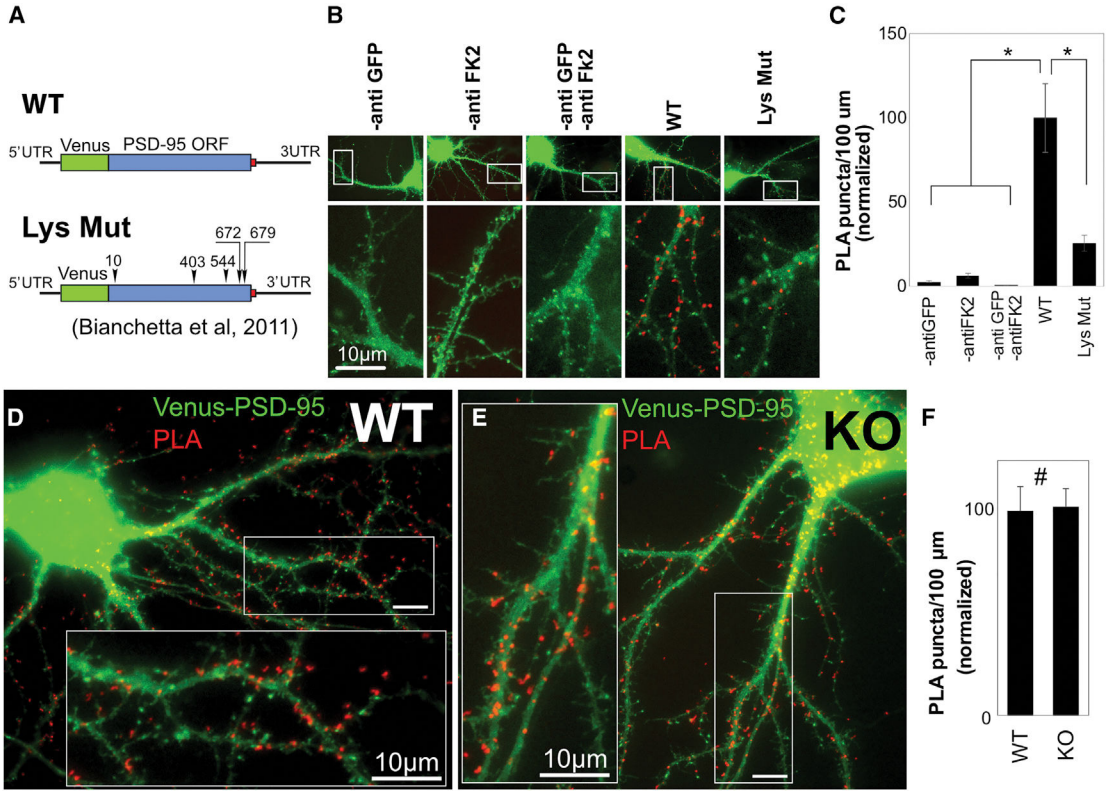

Figure 5. Steady-state levels of total ubiquitinated PSD-95 are similar in WT and *Fmr1* KO neurons at 14DIV

(A) Diagram of the Venus-PSD-95 constructs transfected in neurons. Top: Venus-PSD-95 WT; bottom: Venus-PSD-95 Lys Mut.

(B) Representative images of a PLA proof-of-principle experiment using antibodies against GFP (which recognize Venus) and antibodies against ubiquitinated proteins (FK2 clone). Scale bar, 10 µm.

(C) Quantification of a PLA proof-of-principle experiment. Technical negative controls and a biological control (Lys Mut PSD-95) show a dramatic reduction in PLA signal in comparison with WT PSD-95, as expected (one-way ANOVA, $F(4,63) = 10.96$, $p = 0.000$, Tukey HSD *post hoc* comparisons of WT with technical negative controls and biological negative control; $n \geq 9$ cells per condition, from one culture).

(D and E) Representative images of a PLA analysis of total ubiquitinated Venus-PSD-95 in 14 DIV hippocampal neurons. €neurons, (E). *Fmr1* KO neurons. Green, Venus Fluorescent Protein; Red, PLA signal. Scale bar, 10 µm. White boxes show the magnified areas.

(F) Representative experiment in which PLA signal in 14 DIV WT and *Fmr1* KO hippocampal neurons was quantified ($n = 3$, at least 16 neurons per condition per experiment, t test, $p > 0.25$). Data are represented as means ± SEM. *$p < 0.05$, # not significant.

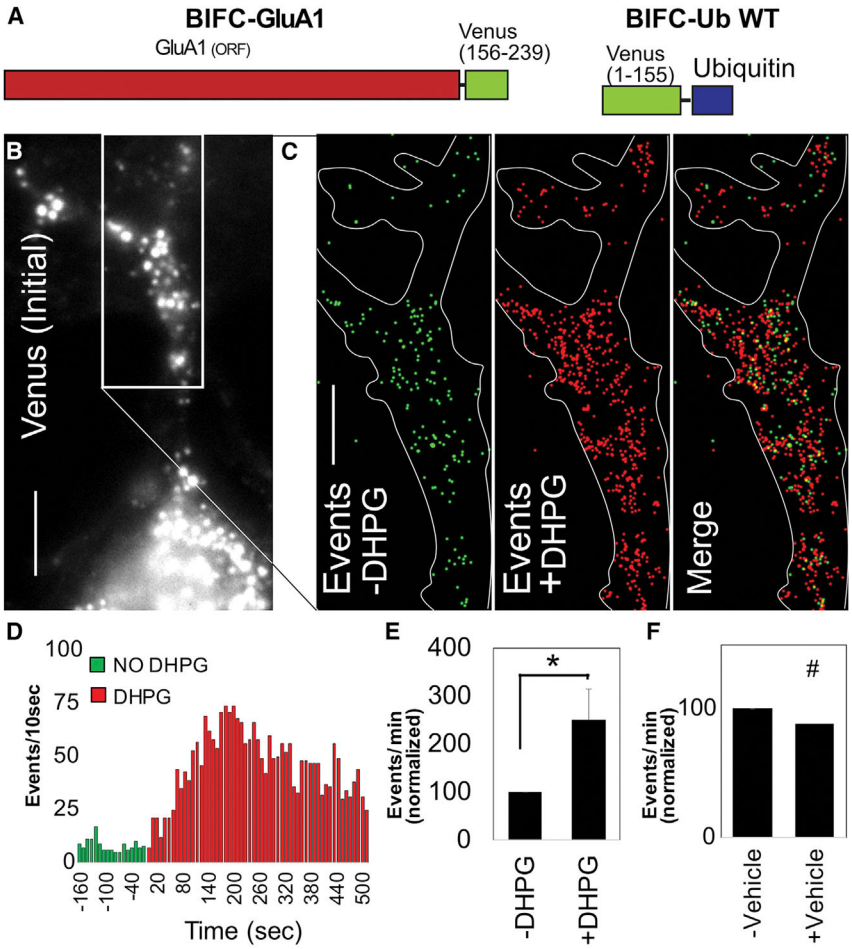

Figure 6. GluA1 ubiquitination rate rapidly increases after stimulation of mGlu receptors

(A) Diagram of the BIFC-GluA1 and BIFC-Ub WT constructs, used for GluA1 ubiquitin mediated fluorescence complementation (UbFC).

(B) Image of a 14DIV hippocampal neuron in which mGlu receptors were stimulated with DHPG, and SM-UbFC for GluA1 was performed. White box indicates the region shown in (C). Scale bar, 10 μm.

(C) Inset of the box shown in (B). Event map showing the GluA1 SM-UbFC events before DHPG (Green), after DHPG (Red) and merged (Green and Red). Scale bar, 5 μm.

(D) Event schedule showing the GluA1 UbFC rate before DHPG (Green) and after DHPG (Red).

(E) After stimulation of mGluR with DHPG, the GluA1 SM-UbFC event rate increased compared with before DHPG (n = 6 neurons from four different cultures, t test, $p < 0.05$, *significant).

(F) After addition of vehicle, the GluA1 UbFC event rate did not change compared with before vehicle (n = 4 neurons, from two different cultures, t test, $p > 0.75$). Data are represented as means ± SEM. *$p < 0.05$, # not significant.

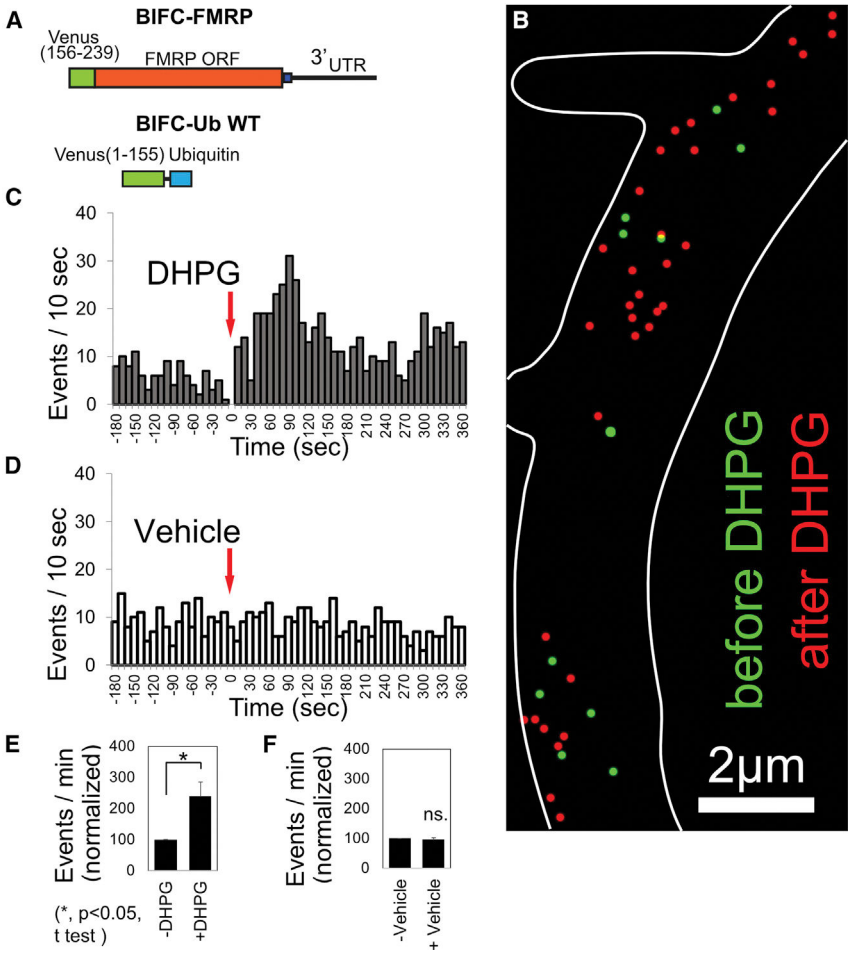

Figure 7. FMRP ubiquitination rate rapidly increases in dendrites after stimulation of mGlu receptors

(A) Diagram of the BIFC-FMRP and BIFC-Ub WT constructs used for FMRP single-molecule ubiquitin mediated fluorescence complementation (SM-UbFC).

(B) Event map of a representative 14DIV hippocampal neuron showing the FMRP UbFC events before DHPG (Green) and after DHPG (Red). Scale bar, 2 µm.

(C) Event schedule showing the FMRP SM-UbFC rate change after treatment with DHPG.

(D) Event schedule showing the FMRP SM-UbFC rate change after treatment with vehicle.

(E) Stimulation of mGluRs with DHPG leads to an increased in FMRP ubiquitination rate (n = 6 neurons from five different cultures, t test, $p < 0.05$, *significant).

(F) In contrast, treatment with vehicle leads to no increase in FMRP ubiquitination rate (n = 3 neurons from two different cultures, t test, $p = 0.48$). Data are represented as means ± SEM. *$p < 0.05$, # not significant.

KEY RESOURCES TABLE

REAGENT or RESOURCE	SOURCE	IDENTIFIER
Antibodies		
Anti GFP (chicken)	Aves Labs, Tigard, OR	Aves Labs Cat# GFP-1010, RRID:AB_2307313
Anti-20S Proteasome Core Subunits Rabbit pAb	Milipore, Billerica, MA	Millipore Cat# ST1053-100UL, RRID:AB_437908
Alexa Fluor® 488 AffiniPure Donkey Anti-Chicken IgY (IgG) (H + L)	JacksonImmunoResearch Laboratories, West Grove, PA	Jackson ImmunoResearch Labs Cat# 703-545-155, RRID:AB_2340375
Donkey anti-Rabbit, Alexa 546 conjugate	Waltham, MA	Thermo Fisher Scientific Cat# A10040, RRID:AB_2534016
Anti-PSD95 antibody (ab18258), rabbit polyclonal,	Abcam, Cambridge, United Kingdom	Abcam Cat# ab18258, RRID:AB_444362
Anti-Ubiquitinylated proteins Antibody, clone FK2	Milipore, Billerica, MA	Millipore Cat# 04-263, RRID:AB_612093
Anti-PSD-95 antibody (clone K28/43), mouse monoclonal	NeuroMab	NeuroMab, Antibodies inc. 75-028, RRID: AB_2292909
HA-Tag (C29F4) rabbit polyclonal	Cell Signaling	Cell Signaling, mAb #3724, RRID: AB_1549585
ChromoTek RFP Monoclonal antibody, mouse monoclonal	ChromoTek	ChromoTek, 6g6, RRID: AB_2631395
Anti-GAPDH hFAB™ rhodamine antibody, human FAB, one-step detection	BioRad	BioRad, #12004167
IRDye® 800CW Donkey anti-Rabbit IgG Secondary antibody	Li-COR	Li-COR, 926-32213 RRID: AB_621848
IRDye® 680LT Donkey anti-Mouse IgG Secondary antibody	Li-COR	Li-COR, 926-68022, RRID: AB_10715072
HRP Goat Anti-Mouse IgG (H + L)	ABclonal	ABclonal, AS003, RRID: AB_2769851
HRP Goat Anti-Rabbit IgG (H + L)	ABclonal	ABclonal, AS014, RRID: AB_2769854
GFP-Trap® Magnetic Particles M-270, alpaca monoclonal nanobody	ChromoTek	ChromoTek, gtma, RRID: AB_2631358
Bacterial and virus strains		
One Shot™ TOP10 Chemically Competent *E. coli*	Thermo Fisher	C404006
Chemicals, peptides, and recombinant proteins		
(S)-3,5-DHPG	Tocris	Cat. No. 0805
B-27™ Supplement (50X), serum free	Thermo Fisher Scientific	Cat. No. 17504044
Neurobasal Medium	Thermo Fisher Scientific	Cat. No. 21103049
DMEM, high glucose	Thermo Fisher Scientific	Cat. No. 11965092
Hibernate E low fluorescence	BrainBits	HELF
Poly-D-lysine hydrobromide	Millipore	P6407-5MG

REAGENT or RESOURCE	SOURCE	IDENTIFIER
Corning™ Donor Horse Serum, U.S. Sourced	Fisher Scientific	Cat. No. MT35030CV
TERGITOL	Sigma-Aldrich	CAS Number 127087-87-0
Triton™ X-100 Surfactant	Sigma-Aldrich	CAS Number 9002-93-1
Paraformaldehyde	Sigma-Aldrich	158127
HLI373	Tocris	Cat. No. 3503
PR-619	Sigma-Aldrich	SML0430
Critical commercial assays		
Duolink™ In Situ Red Starter Kit Mouse/Rabbit	Millipore Sigma, St. Louis, MO	DUO92101
Experimental models: Cell lines		
Neuro-2a	Sigma Aldrich, St. Louis, MO	ECACC Cat# 89121404, RRID: CVCL_0470
SY-SH5Y cell line, ATCC	ATCC, Manassas, Virginia	ATCC Cat# CRL-2266, RRID: CVCL_0019
Experimental models: Organisms/strains		
C57BL/6J-	The Jackson Laboratory, Bar Harbor, Maine	IMSR Cat# JAX: 000664, RRID:IMSR_JAX: 000664
B6.129P2-Fmr1 ^{tm1Cgr}/J	The Jackson Laboratory, Bar Harbor, Maine	IMSR Cat# JAX: 003025, RRID:IMSR_JAX: 003025
Oligonucleotides		
Primers for subcloning of plasmids used in this study, see method details, constructs subsection	This paper	N/A
Recombinant DNA		
pUbFC-YN173-Ub	Fang and Kerppola, 2004	N/A
pBiFC-JunCC155	Fang and Kerppola, 2004	N/A
Venus-1-155-Ubiquitin plasmid	This paper	N/A
Venus-1-155-Ubiquitin G76A mutant	This paper	N/A
Venus-1-155-ΔUbiq	This paper	N/A
Venus (156-239)-PSD-95 plasmid	This paper	N/A
Venus (156-239)-PSD-95 lysine mutant	This paper	N/A
Venus-PSD-95	Ifrim et al., 2015	N/A

REAGENT or RESOURCE	SOURCE	IDENTIFIER
Venus-PSD-95 lysine mutant	This paper	N/A
UbFC-GluA1-Venus(156-239)	This paper	N/A
Venus(156-239)-FMRP-3UTR	This paper	N/A
His-Venus	Ifrim et al., 2015	N/A
pcDNA 3.1 (–)	ThermoFisher	V79520
pmScarlet-i_C1	Addgene plasmid # 85044	RRID: Addgene_85044
Software and algorithms		
ImageJ	(Schneider et al., 2012)	https://imagej.nih.gov/ij/
OCTANE ImageJ Plugin	(Tatavarty et al., 2012)	https://health.uconn.edu/yu-lab/software
Other		
Lipofectamine 2000 Transfection reagent	Thermo Fisher Scientific	11668019
QuickChange II XL Site-Directed Mutagenesis Kit	Agilent Technologies, La Jolla, CA	200521
ProLong™ Diamond Antifade Mountant	Thermo Fisher	P36970
PEI MAX 40K	Avantor 75800-188, Polysciences Inc	CAS Number: 49553-93-7
cOmplete™, EDTA-free Protease Inhibitor Cocktail	Roche	04693116001
Pierce BCA Protein Assay Kit	Thermo Fisher Scientific	Cat # 23225
GFP-Trap Magnetic Beads	Chromotek	gtma
Tanon™ High-sig ECL Western Blotting Substrate	(ABclonal)	Cat# 180-5001